NeuroImage 198 (2019) 198–220

Contents lists available at ScienceDirect

NeuroImage

journal homepage: www.elsevier.com/locate/neuroimage

Assessing spatiotemporal variability of brain spontaneous activity by multiscale entropy and functional connectivity

Mianxin Liu [a], Chenchen Song [b], Yuqi Liang [a], Thomas Knöpfel [b,*], Changsong Zhou [a,c,d,e,**]

[a] Department of Physics, Centre for Nonlinear Studies and Beijing-Hong Kong-Singapore Joint Centre for Nonlinear and Complex Systems (Hong Kong), Institute of Computational and Theoretical Studies, Hong Kong Baptist University, Kowloon Tong, Hong Kong
[b] Laboratory for Neuronal Circuit Dynamics, Imperial College London, London, UK
[c] Research Centre, HKBU Institute of Research and Continuing Education, Virtual University Park Building, South Area Hi-tech Industrial Park, Shenzhen, China
[d] Beijing Computational Science Research Center, Beijing, China
[e] Department of Physics, Zhejiang University, 38 Zheda Road, Hangzhou, China

ARTICLE INFO

Keywords:
Brain signal variability
Functional connectivity
Multiscale entropy
Optical voltage imaging
Cortical circuit dynamics

ABSTRACT

Brain signaling occurs across a wide range of spatial and temporal scales, and analysis of brain signal variability and synchrony has attracted recent attention as markers of intelligence, cognitive states, and brain disorders. However, current technologies to measure brain signals in humans have limited resolutions either in space or in time and cannot fully capture spatiotemporal variability, leaving it untested whether temporal variability and spatiotemporal synchrony are valid and reliable proxy of spatiotemporal variability in vivo. Here we used optical voltage imaging in mice under anesthesia and wakefulness to monitor cortical voltage activity at both high spatial and temporal resolutions to investigate functional connectivity (FC, a measure of spatiotemporal synchronization), Multi-Scale Entropy (MSE, a measure of temporal variability), and their relationships to Regional Entropy (RE, a measure of spatiotemporal variability). We observed that across cortical space, MSE pattern can largely explain RE pattern at small and large temporal scales with high positive and negative correlation respectively, while FC pattern strongly negatively associated with RE pattern. The time course of FC and small scale MSE tightly followed that of RE, while large scale MSE was more loosely coupled to RE. fMRI and EEG data simulated by reducing spatiotemporal resolution of the voltage imaging data or considering hemodynamics yielded MSE and FC measures that still contained information about RE based on the high resolution voltage imaging data. This suggested that MSE and FC could still be effective measures to capture spatiotemporal variability under limitation of imaging modalities applicable to human subjects. Our results support the notion that FC and MSE are effective biomarkers for brain states, and provide a promising viewpoint to unify these two principal domains in human brain data analysis.

1. Introduction

An astonishing feature of the mammalian cortex is the ubiquitous variability in the spatiotemporal dynamics of its activity. This variability emerges from the signaling between individual neurons and neuronal circuits (Stein et al., 2005; Faisal et al., 2008) that occurs over broad temporal and spatial scales (Avena-Koenigsberger et al., 2018; Muller et al., 2018) and is hypothesized to reflect a crucial working principle of cortical circuit activity - self-organized criticality (Bak et al., 1987; Shew and Plenz, 2013; Cocchi et al., 2017; Palva and Palva, 2018). When the system approaches critical-state dynamics, the variability of spatiotemporal patterns of cortical activities, which can be measured by regional entropy (RE) and interpreted as information capacity, is maximized (Shew et al., 2011). Modelling studies suggested this critical state of the brain requires a well-tuned balance between synaptic excitation and inhibition (Shew et al., 2009, 2011; Yang et al., 2017). At criticality, multiple functional features such as dynamic range (Shew et al., 2009), information transfer (Shew et al., 2011), and energy-efficiency (Yang et al., 2017) are optimized. Recordings from neuronal cultures, anaesthetized rodents and awake monkeys indicated that RE decreases with

* Corresponding author.
** Corresponding author. Department of Physics, Centre for Nonlinear Studies and Beijing-Hong Kong-Singapore Joint Centre for Nonlinear and Complex Systems (Hong Kong), Institute of Computational and Theoretical Studies, Hong Kong Baptist University, Kowloon Tong, Hong Kong
E-mail addresses: tknopfel@knopfel-lab.net (T. Knöpfel), cszhou@hkbu.edu.hk (C. Zhou).

https://doi.org/10.1016/j.neuroimage.2019.05.022
Received 30 January 2019; Received in revised form 17 April 2019; Accepted 9 May 2019
Available online 12 May 2019

manipulations that drive circuit dynamics away from criticality (Shew et al., 2011; Fagerholm et al., 2016).

These basic findings motivate the use of measures of variability in spatiotemporal dynamics of the brain as biomarkers for human brain functional states (see reviews Garrett et al., 2013; Takahashi, 2013; Mashour and Hudetz, 2018). Reliably measuring the spatiotemporal variability requires data acquisition with sufficient spatiotemporal resolution, but existing technologies to measure human brain activity are limited either in spatial or temporal resolution, raising concerns whether they capture spatiotemporal variability with sufficient precision. For example, clinical electrophysiological data using approaches such as scalp electroencephalogram (EEG) have high temporal resolution but limited spatial resolution. Functional magnetic resonance imaging (fMRI) measures brain activities based on blood oxygen level-dependent (BOLD) fluctuations with good spatial resolution but low temporal resolution. Thus, the analysis of spatiotemporal patterns and the development of variability-based biomarkers have so far been focused on either spatial or temporal features of brain signals.

Among the established biomarkers, temporal variability refers to a family of measures that quantify the repertoire of temporal patterns. These biomarkers include classical entropy-based measures (Richman and Moorman, 2000; Pincus, 1991) which give maximal values at uncorrelated random noise. However, biological signals are characterized by long-range autocorrelated fluctuations that appear across multiple temporal scales, which would not be considered as of "high complexity" using classical entropy measures. Multiscale entropy (MSE) uses a coarse graining process and can differentiate between random noise and biological signals (Costa et al., 2002; Courtiol et al., 2016). MSE calculated from EEG recordings in humans has been applied to study brain signal variability in relation to aging and development (McIntosh et al., 2008; Takahashi et al., 2009), functional performance (Heisz et al., 2012), and various mental disorders and brain diseases, including schizophrenia (Takahashi et al., 2010), depression (Okazaki et al., 2013), traumatic brain injury (Beharelle et al., 2012), autism (Bosl et al., 2011; Catarino et al., 2011; Ghanbari et al., 2015), Alzheimer's disease (Mizuno et al., 2010; Escudero et al., 2006; Yang et al., 2013) and its risk gene carriers (Yang et al., 2014).

In fMRI–based studies, functional connectivity (FC) is a widely used and successful measure. FC reduces the spatiotemporal variability to the spatiotemporal synchrony at a very low frequency band, typically measured by the linear correlation of brain signals recorded at pairs of regions of interest. FC can be calculated from relatively short sequences of BOLD signal maps acquired with a slow sampling rate. Accumulating evidence of aberrant neural connectivity in many brain disorders motivates a growing number of studies that apply FC in fMRI to examine possible abnormality in functional interaction in a variety of diseases, including AD (Dennis and Thompson, 2014; Zhang et al., 2010; Ferreira and Busatto, 2013), schizophrenia (Lynall et al., 2010), autism (Assaf et al., 2010), and depression (Mulders et al., 2015), see a recent review (Fornito et al., 2015).

Although MSE is predominantly applied to EEG data and FC to fMRI data, there have been attempts to quantify temporal variability via MSE measures from fMRI data (McDonough and Nashiro, 2014; Grandy et al., 2016; Wang et al., 2018) and spatial variability via advanced FC measures from EEG data (Schoffelen and Gross, 2009; Sakkalis, 2011; Miskovic and Keil, 2015; Kuntzelman and Miskovic, 2017). However, within the broader community of researchers, MSE and FC have mainly been separately developed and applied as proxies of spatiotemporal variability. The different measurement modalities used to achieve either a high spatial or a high temporal resolution complicated cross validation of the two approaches when assessing neuronal spatiotemporal variability.

Optical voltage imaging using genetically encoded voltage indicators (GEVIs) enables the direct monitoring of electrical signaling across large portions of the dorsal cerebral cortex of mice (Akemann et al., 2010, 2012). Taking advantage of its high spatial and temporal resolutions, we used GEVI-based voltage imaging data to investigate the performance of FC and MSE in reflecting features of RE in different cortical structures, temporal variations of RE in ongoing brain activity, and difference of RE across brain states. We found that in different brain regions across the cortex, MSE at small and large scales showed high positive and negative correlations to RE respectively, and FC reflected RE with a negative correlation. Fluctuations of FC and small scale MSE over the observation time reflected RE variations with significant negative and positive correlation respectively, while large scale MSE changes loosely coupled to RE changes with a negative correlation. These RE-small scale MSE and RE-FC relationships were robust across brain states of anesthesia and wakefulness. Under simulated resolution of human neuroimaging, these relationships were weakened but maintained significant unless the spatiotemporal information was severely reduced.

Our study provides an integrated understanding of the two previously disconnected applications of FC in fMRI and MSE in EEG-based approaches, and hence offers confidence for the applications of MSE and FC as biomarkers for the investigations of brain functions in healthy and diseased human subjects using EEG and fMRI.

2. Materials and methods

2.1. GEVI-based optical voltage imaging using transgenic mice

All regulated procedures were in accordance with the UK Animal Scientific Procedures Act (1986) under Home Office Project and Personal Licenses following appropriate ethical review.

Voltage imaging was performed as described in (Akemann et al., 2010, 2012; Scott et al., 2014). Briefly, 5 transgenic mice expressing the genetically encoded voltage indicator (GEVI) chimeric VSFP Butterfly (Mishina et al., 2014; Song et al., 2018) in pyramidal neurons across all cortical layers (CaMK2A-tTA; tetO-chiVSFP) were used. Fluorescence intensities of the chimeric VSFP Butterfly voltage indicator's FRET donor and acceptor fluorescent proteins decrease and increase, respectively, with membrane depolarization. Hence, the ratio of acceptor- and donor fluorescence reports membrane voltage changes and is (at least nominally) independent of indicator concentration. The epifluorescence imaging approach we used here restricts optical access and signal detection to the superficial cortical layers.

Under surgical anesthesia, all animals were implanted with a transcranial cortical window through a thinned but otherwise fully intact skull and a head-fixation post.

Image acquisition was performed using a dual emission widefield epifluorescence macroscope equipped with two synchronized CMOS cameras, using high power halogen lamps for fluorescence excitation (Moritex, BrainVision) and the following optics (Semrock): mCitrine (donor) excitation 500/24, mCitrine emission FF01-542/27, mKate2 (acceptor) emission BLP01-594R-25, excitation beam splitter 515LP, and detection beam splitter 580LP. The voltage signals were computed from the ratio (R) between the acceptor and donor fluorescence ($F_{acceptor}$, F_{donor}, acquired with the two cameras, $R = F_{acceptor}/F_{donor}$), as $\Delta R/R = (R(t) - R_{mean})/R_{mean}$ (Akemann et al., 2010, 2012). Contamination of the voltage signals by optical signals caused by blood volume and oxygenation changes (known to be associated with neuronal activity) was minimized by signal gain equalization as described in Akemann et al. (2012).

The datasets were acquired at 150 Hz acquisition frame rate with cortex-wide two-hemisphere field of view. During the imaging session, trials of 180s duration were acquired as mice gradually recovered from 40 mg/kg pentobarbital sodium sedation towards wakefulness. Spatial resolution of the optical system is 66 × 66 μm per pixel, which captured activities from approximately 400 neurons according to the estimation of neuron density in mouse cortex (Keller et al., 2018) and assuming cortical thickness as 1 mm.

The level of anesthesia was monitored using the heart rate as a proxy (Lecci et al., 2017). A brain state characterized by an absolute lack of spontaneous limb and whisker movements and heart rate below 9 Hz is indicated as "anesthesia". The state where the animal recovered from

anesthesia with occasional spontaneous body movements and whisking is indicated as "wakefulness". Based on these criteria, two trials were chosen for each mouse, one for the state of anesthesia and one for wakefulness.

2.2. Data preprocessing

Detailed methods to extract voltage signal from raw fluorescence signals were as described (Akemann et al., 2013; Shimaoka et al., 2017). Parameters for digital filters were optimized to exclude noise while preserving the high spatial-temporal resolution of the data as much as possible. In all datasets, we used 0.5 Hz high-pass temporal filtering (Chebyshev Type II, function *imfilter*, MATLAB, Mathworks Inc, USA) for improving signal-to-noise ratio and detrending. Periods with large fluctuations (amplitude > mean + 3 std) of the filtered voltage signal were identified as movement artefacts and excluded from the analysis.

2.3. The seed region, binary patterns and the regional entropy

Regional entropy (RE) measures spatiotemporal pattern variability to quantify the repertoire size of population activity within a spatial region over time and the information capacity within the datasets (Shew et al., 2011; Fagerholm et al., 2016). To compute RE, we first defined a seed region as a square window of $d \times d$ pixels. Seed regions that contain pixels outside the boundary of the imaged cortex were excluded from calculations. RE was then calculated based on the d^2 signals within each seed regions covering the imaged mouse cortex.

Within seed region, we generated binary patterns by defining binary events for every time series x_t, according to the standard deviation above mean value:

$$B_t = \begin{cases} 0 & (if\, x_t < mean + 1\ std\ ) \\ 1 & (if\, x_t \geq mean + 1\ std\ ). \end{cases}$$

Note that within $d \times d$ seed region the binary pattern corresponds to a d^2 bits binary number, which can be further converted into a decimal number pattern label, varying within a range between 0 to 2^{d^2}. This pattern labelling process of RE is demonstrated in Fig. 1 (a).

Finally, RE was calculated as the Shannon entropy from the probability p_i of occurrence of the i-th pattern,

$$RE = -\sum_i p_i \log(p_i).$$

Results obtained with $d = 5$ (330 μm) were used for illustrations; The effect of window size is shown in Appendix Fig. A10. Conclusions hold for window sizes of 3, 5 and 7.

2.4. Multiscale entropy

Brain signals usually show structured fluctuations across multiple temporal scales and exhibit long-range correlations and non-linearity. Multiscale entropy (MSE) and its variations were designed to detect these properties in empirical data (Costa et al., 2003; Azami et al., 2017; Li et al., 2010; Shi et al., 2017).

Here we specifically used a developed version of MSE named multiscale dispersion entropy for its computational efficiency (Azami et al., 2017). The original MSE (Costa et al., 2002) is computed using sample entropy, with a high computational load ($O(N^2)$). Dispersion entropy is related to sample entropy, but it is more tolerant to the presence of noise in time series and can significantly reduce the computation time ($O(N)$). MSE calculations using either sample entropy or dispersion entropy yielded similar results when applied to neural time series data (Kuntzelman et al., 2018). In this paper, MSE refers to multiscale dispersion entropy.

The calculation of multiscale dispersion entropy involves (i) coarse-graining the original signal into different temporal scales, and (ii) computing the dispersion entropy in the coarse-grained signal. Coarse-graining is performed by binning the original signal $X = \{x_1, x_2, \ldots, x_t\}$ and calculating the mean value inside the bins of length s to generate a new series Y^s,

$$y_j^s = 1/s \sum_{k=(j-1)s+1}^{js} x_k, \quad 1 \leq j \leq N/s.$$

The length of the bin, s, is called the scale factor.

Dispersion entropy discovers the symbolic dynamics (or dispersion patterns) in a time series, and then uses Shannon entropy from the distribution of pattern appearance probability to quantify signal uncertainty. We computed the dispersion entropy for each new series Y^s. An illustration of the major computation steps is shown in Fig. 1 (b). First, every element of the time series of measurements is mapped to one of the

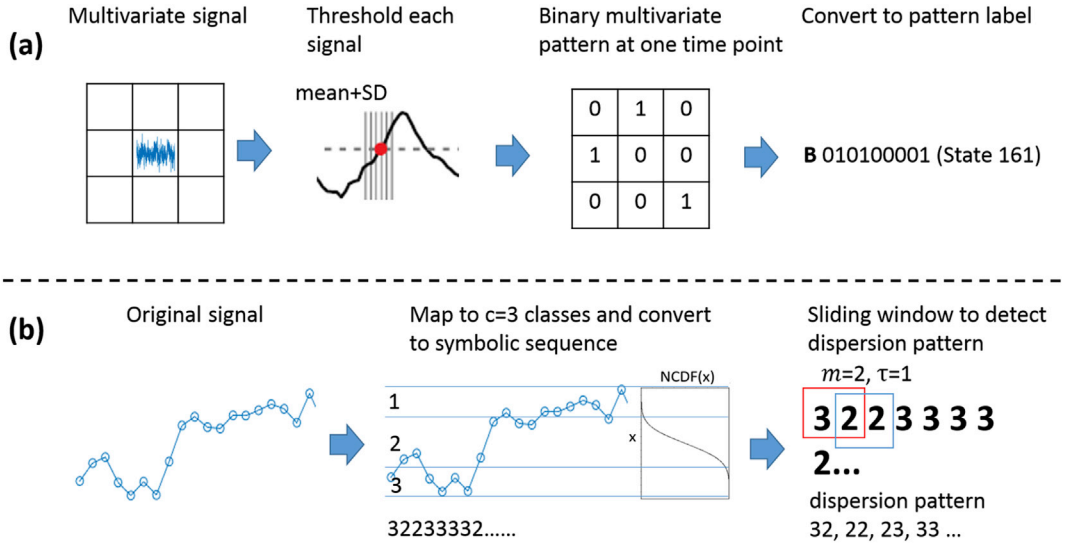

Fig. 1. Schematics of the pattern-labelling algorithm for regional entropy (RE) and multiscale dispersion entropy (MSE). (a) Pattern labelling process for regional entropy for the case of 3 × 3 seed region (NB: In this study 5 × 5 was used). (b) An illustration of the dispersion pattern detection in dispersion entropy with $c = 3$, $\tau = 1$ and $m = 2$. (NB: In this study $c = 6$ was used) For both RE and MSE, entropy was calculated after pattern labelling using Shannon entropy of the probability distribution of the pattern appearance.

c classes (a label z_i whose value ranges from 1 to c) using the normal cumulative distribution function (NCDF), through two steps of mapping,

$$\theta_i = 1/D\sqrt{2\pi}\int_{-\infty}^{x_i} exp\left(-(x-M)/2D^2\right)dx,$$

followed by,

$$z_i = round(c^*\theta_i + 0.5).$$

The mean M and standard derivation D of the NCDF were defined by the mean and standard deviation of the original signal X, and fixed constant across all coarse-grained scales. This is similar to the "tolerance" parameter in previous MSE calculations (Costa et al., 2002). Next, a sliding window of length m (also called "embedding dimension") and step length τ (also called "time delay") was used to count the frequency of each c^m potential dispersion patterns. Finally, the probability of each of these dispersion patterns is used to calculate the Shannon entropy. Theoretically, the maximum value of dispersion entropy occurs when the signal is completely random where all dispersion patterns can exist with equal probability, while the smallest possible value is obtained when signal is periodic and there is only a single dispersion pattern (Azami et al., 2017; Rostaghi and Azami, 2016).

We used the recommended parameters of $c = 6$, $\tau = 1$, and $m = 2$ (Azami et al., 2017; Rostaghi and Azami, 2016) for all our analyses presented.

The MSE values computed for each pixel within one seed region were averaged to compare with the corresponding RE of the same seed region.

2.5. Functional connectivity

Functional connectivity (FC) measures the spatial correlation between pairs of time series, and FC strength reflects spatiotemporal synchronization. For each pixel, correlations between the pixel signal and time-series of all other pixels on the imaged cortical regions were computed, and their absolute values (negative correlation accounting for out-of-phase synchrony) were averaged to obtain a FC value. This FC value describes the strength of synchrony between the signal from one pixel and the global signal.

The independently calculated FC values from each pixel within the $d \times d$ pixels seed region were averaged for the comparison with RE of the same region.

2.6. Signal resolution simulation

To simulate MSE and FC computations under conditions of data acquisition with reduced resolution, we decreased the resolution of our datasets in either the temporal or spatial domains via smoothing.

To simulate a reduced spatial resolution, we used Gaussian spatial smoothing on our voltage imaging data with different kernel standard deviations (function *imgaussfilt* in MATLAB R2016a, Mathworks Inc, USA). Standard deviation of the Gaussian kernel, σ, determines the smoothing strength, where a larger σ leads to lower spatial resolution.

To simulate a reduced temporal resolution, we used a temporal band pass filter with upper bound as reported in the Results section. Lower bound was kept to 0.5 Hz.

2.7. Transformation of neuronal membrane voltage signals into simulated BOLD signals

The exact relationship between neuronal membrane voltage and the BOLD signals measured with fMRI is an unresolved matter of debate (Bandettini, 2014). Despite being admittedly over simplistic, much fMRI work is based on the BOLD-neural activity relationship established by Logothetis et al. (2001). This relationship can be simulated by convolution of the electrical signals with a response function that implements temporal averaging and delay (https://www.frontiersin.org/articles/10.3389/fnhum.2013.00034/full Mukamel et al., 2005; https://www.frontiersin.org/articles/10.3389/fnhum.2013.00034/full Nir et al., 2007; https://www.frontiersin.org/articles/10.3389/fnhum.2013.00034/full Privman et al., 2007). The response function (Fig. 2) was generated by Statistical Parametric Mapping (SPM) toolbox using the default setting (6 s delay of response peak, 16 s delay of undershoot, 32 s length of kernel). The designed kernel lasts for 32 s and thus integrates over the past 32 s of voltage signal to generate one point of BOLD signal. The convolution started at 32 s after the voltage signal recording onset to avoid convolution without voltage signal. When comparing BOLD and optical voltage signals, we excluded the voltage signals within the first 32 s, simulating simultaneously recorded BOLD and voltage signals. The resulting BOLD signal was down-sampled to 1 Hz to simulate the sampling rate of practical fMRI.

2.8. Statistical analysis

The correlation analysis was done with the algorithms implemented in MATLAB R2016a (function *corrcoef*, Mathworks Inc, USA). Wilcoxon signed rank test was used in the group comparison to examine the significance in difference between anesthesia and wakefulness states.

To control the false discovery rate (FDR) in multiple testing and comparisons, the obtained p-values were pooled together and adjusted via the Benjamini-Hochberg method (function *p.adjust* in R-language) at FDR = 0.05 level. The set of p-values gone through correction were stated

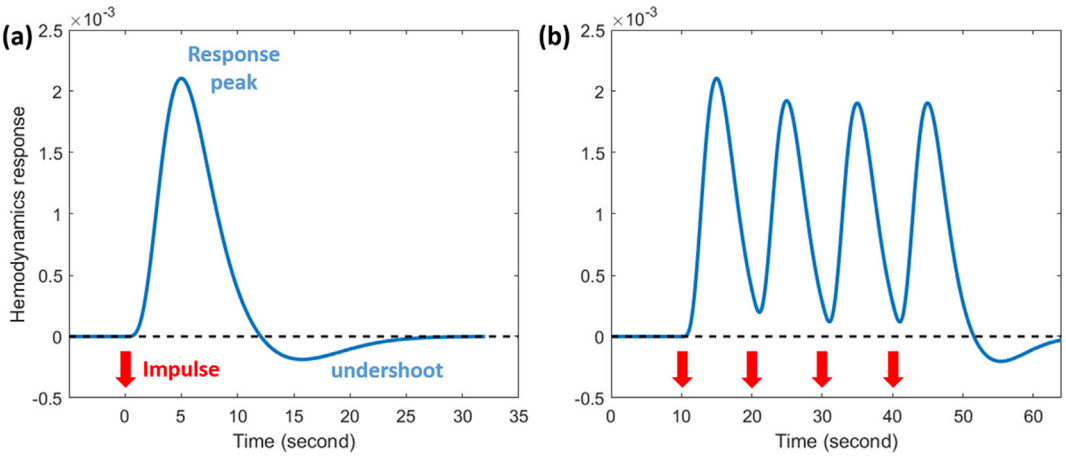

Fig. 2. Illustration of the simulated BOLD signal in response to a membrane voltage impulse. (a) By a single impulse (Dirac pulse, delta function). (b) By multiple impulses.

in the figure caption. The adjusted p values were required to be less than 0.05 to support the significance of discovered correlations or differences.

3. Results

3.1. FC and MSE detect RE changes in space and time

To see whether FC and MSE can reflect the RE difference across the cortex, we first computed RE, FC, MSE in different seed regions across the imaged cortex using the full-length voltage signals for each recording from wakeful mice. The resulting spatial distribution of RE (Fig. 3(a)), FC (Fig. 3(b)), and MSE at small scale ($s = 1$; Fig. 3(c)) and large scale ($s = 20$; Fig. 3(d)) are shown for mouse #1 in the wakefulness state. RE values differed across the cortex, with higher RE values in the prefrontal areas and lower near the posterior regions (Fig. 3 (a)). Compared with RE, the spatial map of FC is largely reversed along the frontal-posterior axis (Fig. 3 (b), (e); RE-FC $r = -0.728$, $p < 0.001$, mouse #1), and this is also observed at the group level (Fig. 3 (g)). The small scale MSE spatial map resembles the RE map (Fig. 3 (c), (f); RE-small scale MSE $r = 0.973$, $p < 0.001$, mouse #1) while the large scale MSE map was reversed (Fig. 3 (d), (f); RE-large scale MSE $r = -0.939$, $p < 0.001$, mouse #1). For other mice, the MSE-RE region-wise correlation systematically vary with MSE scale, where the correlation coefficients change from positive values being close to 1 at small scales to negative values close to −1 at large scales (Fig. 3 (g)).

RE of spontaneous brain activity fluctuates across sequential time

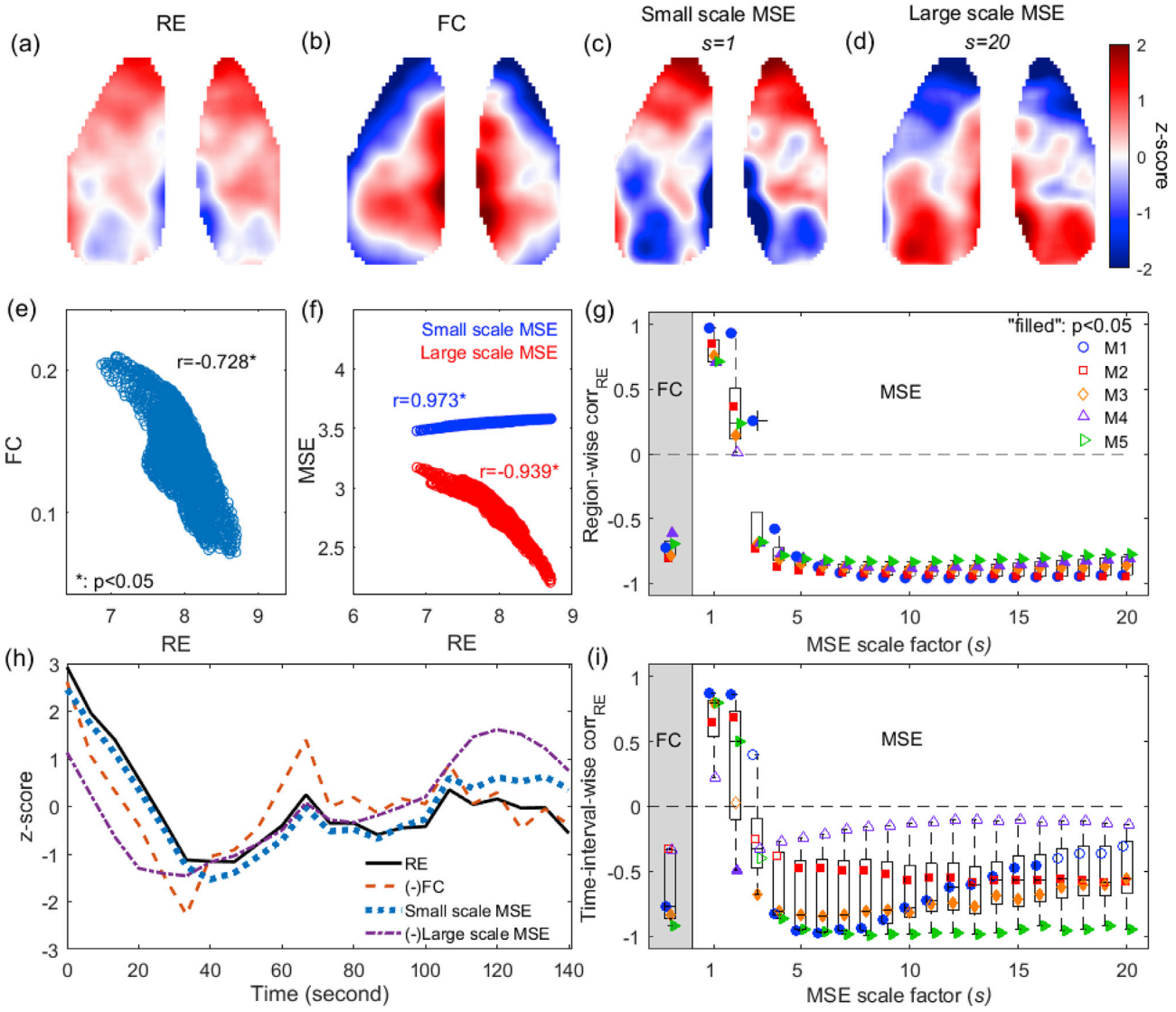

Fig. 3. MSE and FC correlates with spatial and temporal patterns of RE in wakefulness brain states. (a–c) The spatial maps of (a) RE, (b) FC, (c) small scale MSE ($s = 1$) and (d) large scale MSE ($s = 20$) calculated from 180s voltage imaging at 150 Hz in mouse #1. (e) Cortex-wide region-wise correlation of RE-FC strength using data from (a) and (b). (f) Cortex-wide region-wise correlation of RE-small scale MSE (blue) and RE-large scale MSE (red) using data from (a), (c) and (d). (g) The scatter plot and box plot of RE-FC correlation (left, grey) and RE-MSE correlations over 20 scales (right) from 5 mice in the wakeful group. The p-values from 105 plotted correlations were corrected together. Filled data points show $p < 0.05$. Box plots show median (line inside box), 25th and 75th percentiles (box edges), the most extreme data points excluding outliers (whiskers), and any individual outliers ('+' symbol). (h) Z-score showing the temporal evolution of the spatial average across all seed regions for RE, FC, small scale MSE and large scale MSE for mouse #1. Each time point was the spatial average value of RE, FC, MSE calculated within a sliding window of 33s (26s overlap). The time axis shows the onset time of corresponding time window. The values of FC and MSE $s = 20$ were multiplied by −1 for illustration of evolution trends with RE. (i) RE-FC and RE-MSE correlations in the temporal evolutions from the wakefulness group. The p-values in (i) were corrected together. Individual analyses of the other 4 mice are shown in Appendix Figs. A1-A4. * indicates p-values < 0.05.

windows, hence we next tested whether FC and MSE can track RE along temporal evolution. Co-variations of spatial average of RE, FC and MSE values across all seed regions revealed that FC and small scale MSE tightly follow the temporal fluctuations of RE (Fig. 3 (h)). However, large scale MSE only approximates the trend of RE variation and does not reflect detailed small fluctuations. This observation is less influenced by the selection of window size (Fig. A11). FC-RE correlations were all negative in the group level (Fig. 3 (i)), and the ability of MSE to reflect RE in temporal evolution decreases with increasing MSE scale size, as reflected by the MSE-RE correlations (Fig. 3 (i)). Interestingly, additional analysis showed that even though the temporal variation of RE, FC and MSE would not perfectly reflect each other, the spatial maps from the same time window are more similar (see Appendix Fig. A12). This suggests that the FC/MSE correlations to RE across cortex and time evolution are somewhat independent and respectively related to the capability to reflect spatial and temporal variabilities.

3.2. FC and MSE performance in anaesthetized state

FC and MSE have been widely applied as biomarkers for analysis of brain activity under different states. We next investigated whether the ability of MSE and FC to reflect RE withstand changes of brain states. Similar to the wakefulness state (Fig. 3), RE and small scale MSE displayed similar spatial patterns (Fig. 4 (a), (c), (f); small scale MSE-RE $r = 0.989$, $p < 0.001$, Mouse #1) while FC (Fig. 4 (e); RE-FC $r = -0.869$, $p < 0.001$, Mouse #1) and large scale MSE (Fig. 4 (a), (b), (d), (f); large scale MSE-RE $r = -0.941$, $p < 0.001$) generated inverted spatial maps. At the group level, MSE-RE correlation transitioned from positive to negative values with increasing scale size (Fig. 4 (g)). Similar to observations during wakefulness (Fig. 3), under anaesthetized state, FC and small scale MSE reflects RE through temporal evolution, but RE is not well-captured by large scale MSE (Fig. 4 (h)). Thus, in our dataset, the qualitative FC-RE and small scale MSE-RE correlations withstand changes

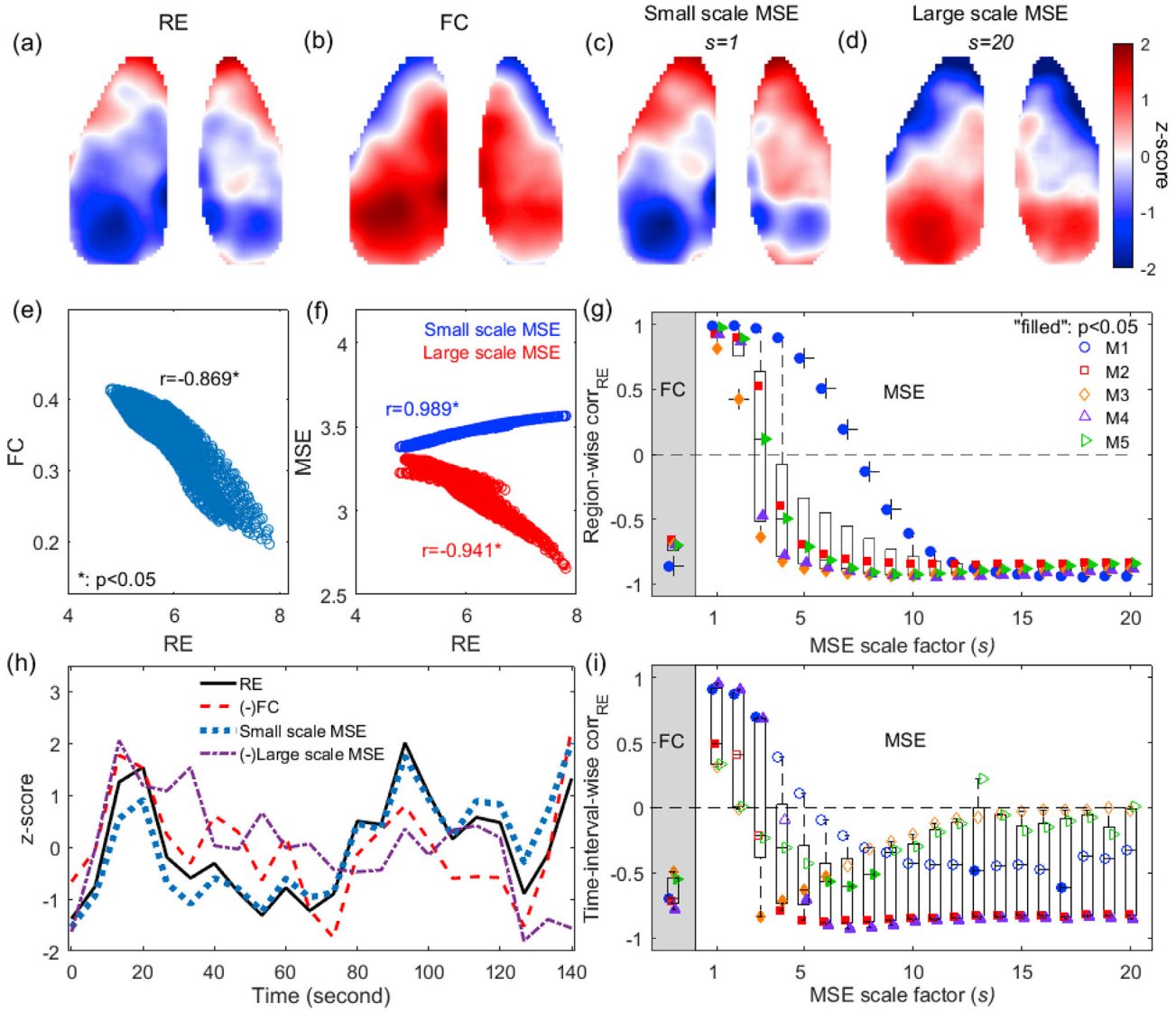

Fig. 4. RE-assessment by MSE and FC in anaesthetized brain state. (a–c) Spatial maps of (a) RE, (b) FC, (c) small scale MSE ($s = 1$) and (d) large scale MSE ($s = 20$) calculated from the full-length voltage signals in exemplified mouse #1 under anaesthetized state. (e) Cortex-wide seed-region-wise correlation of RE-FC strength using data from (a) and (b). (f) Cortex-wide region-wise correlation of RE-small scale MSE (blue) and RE-large scale MSE (red) using data from (a), (c) and (d). (g) The scatter plot and box plot of RE-FC correlation (left side) and RE-MSE correlations over 20 scales (right side) from 5 mice in anesthesia group. The p-values in (g) were corrected together. (h) Temporal evolution of the cortex-wide average values of RE, FC, small scale MSE and large scale MSE for mouse #1 under anaesthetized state. (i) The scatter plot and box plot for RE-FC and RE-MSE correlations temporal evolutions from the anesthesia group. The p values in (i) were corrected together. Individual analyses of the other 4 mice are shown in Appendix Figs. A5-A8.

of brain states (anesthesia vs wakefulness), but large scale MSE-RE correlation could be sensitive to brain states (level of anesthesia in the present data).

3.3. Group level comparisons across brain states

MSE and FC may serve as biomarkers if they can detect spatiotemporal dynamics differences between different brain states within a subject. To demonstrate this, we calculated the cortex-wide average RE, FC and MSE from the full-length (180s) voltage imaging data. We observed negative RE-FC correlations across individuals (Fig. 5 (a); $r = -0.803$, $p = 0.106$ for anesthesia, $r = -0.920$, $p = 0.040$ for wakefulness). The 10 scatters are roughly located near a straight line, suggesting that the FC and RE co-vary with changes in brain state (see below). Across individuals, we also observed positive RE-small scale MSE correlations (Fig. 5 (b); $r = 0.989$, $p = 0.004$ for anaesthetized, and $r = 0.931$, $p = 0.043$ for wakefulness) and negative RE-large scale MSE (Fig. 5 (c); $r = -0.818$, $p = 0.109$ for anesthesia, and $r = -0.993$, $p < 0.001$ for wakefulness).

At the group level, we observed a significant global increase in RE (Fig. 5 (d); $p = 0.049$) and decrease in FC (Fig. 5 (e); $p = 0.049$) across anaesthetized and wakefulness states. In MSE, significant increase showed at scale 1 and significant decrease appeared at larger scales (Fig. 5 (f)).

3.4. FC and MSE performance under limited resolutions of human neuroimaging

Our observations so far pointed towards a possible holistic interpretation of FC-based and MSE-based analysis approaches in human neuroimaging studies. However, preclinical and clinical studies in humans are usually subject to technical constraints of the applicable imaging modalities that are difficult to compare as their spatial and temporal resolutions are divergent: The BOLD signal in fMRI is a proxy for temporally averaged (in the order of 1 s) electrical signaling (in high-resolution fMRI at submillimeter spatial resolution), while EEG is routinely acquired at kHz sampling rates but suffers from low effective spatial resolution due to current spread. To investigate the applicability of the present results to human neuroimaging studies, we manipulated the resolution of the data from the wakefulness condition to a level approximating the spatiotemporal resolution of typical fMRI and EEG recordings in humans. Our aim was to elucidate the effects of reduced temporal or spatial resolution on the measures, and test the robustness of their assessment about spatiotemporal neural variability under conditions of human neuroimaging. We used RE from the full resolution voltage imaging data as a reference for the comparison with MSE and FC re-calculated after resolution reduction. Wakefulness state data were used for this analysis, and results from mouse #1 were shown for

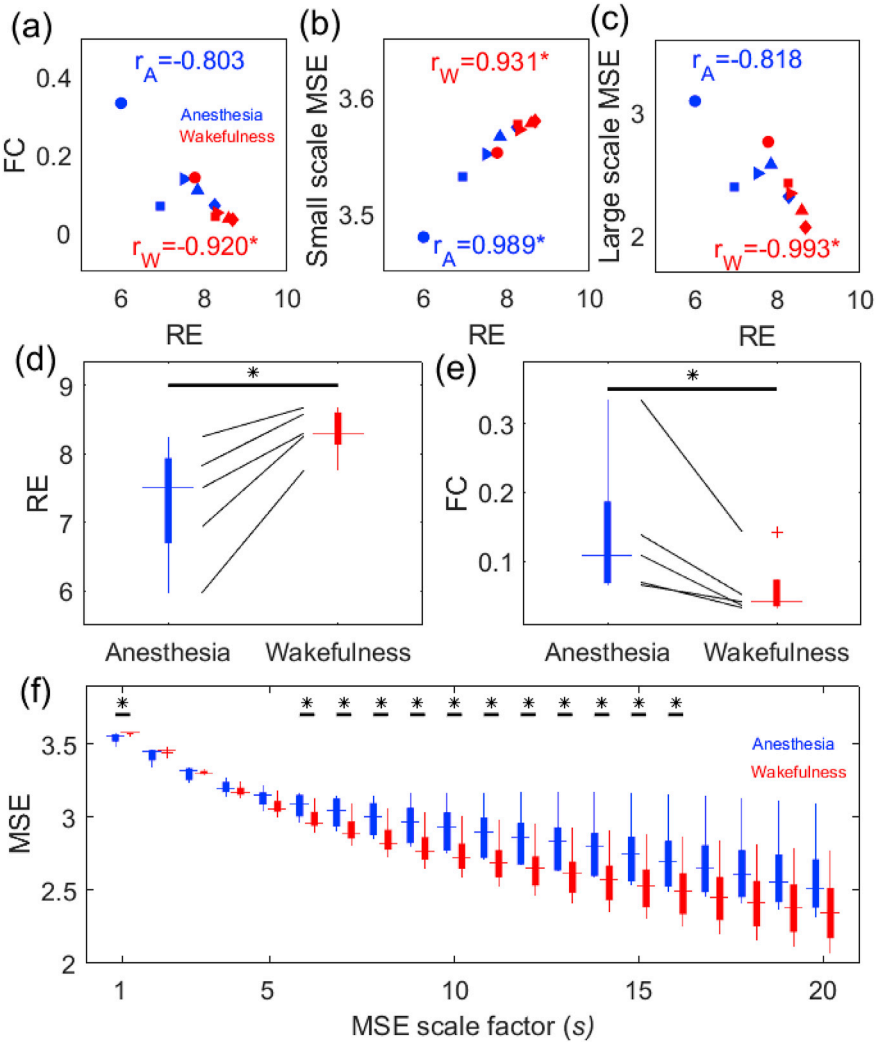

Fig. 5. Group level RE, FC and MSE comparisons across brain states. (a–c) Cortex-wide average (a) RE-FC, (b) RE-small scale MSE, and (c) RE-large scale MSE correlations across anaesthetized and wakefulness states from individual mice (N = 5). (d–e) The box plots and paired ladder plots of cortex-wide RE and FC. (f) The box plots for MSE in anaesthetized and wakefulness conditions. P-values in (d), (e), (f) were corrected. * indicates p-values < 0.05.

illustration.

3.4.1. FC and MSE performance under reduced temporal resolution

To explore the effects of a modest reduction in temporal resolution, we recalculated FC and MSE after temporal bandpass filtering the voltage imaging data at 0.5–50 Hz and at 0.5–25 Hz. In mouse #1, the spatial maps (0.5–25 Hz bandpass filter) of small scale MSE ($s = 1$) and large scale MSE ($s = 20$) largely preserved detailed correspondence to the features of the full resolution RE spatial pattern (Fig. 6 (c), (d)), while the FC map showed a pattern with reduced similarity to the full resolution RE map (Fig. 6 (b)). Temporal filtering caused an overall increase in FC and large scale MSE values and a decrease in small scale MSE values, but the correlation between FC or MSE to RE remains largely unchanged (Fig. 6 (e)-(g)).

In group analysis (Fig. 6 (h)), temporal filtering (0.5–50 Hz and 0.5–25 Hz) introduced minor reduction of the FC-RE negative correlations. For MSE-RE correlation, there is less influence on the positive correlation at small scales and negative correlations at large scales (Fig. 6 (i) and Fig. A9). But the increasing temporal smoothing caused a clear shift of the transition point from positive to negative correlation to a larger MSE scale (Fig. 6 (i)).

FC and MSE still reflected the RE temporal evolution after stronger temporal filtering (0.5–25 Hz; Fig. 6 (j)). The absolute FC-RE correlations strength in time are slightly weakened or increase by temporal filtering (Fig. 6 (k)), but the MSE-RE correlation in time is more profoundly affected. MSE-RE correlation zero-transition point is shifted towards larger scales (Fig. 6 (l)), and the correlation between RE and large scale MSE is gradually decreased (Fig. 6 (l)). The results in individuals demonstrated similar phenomena (Fig. A9).

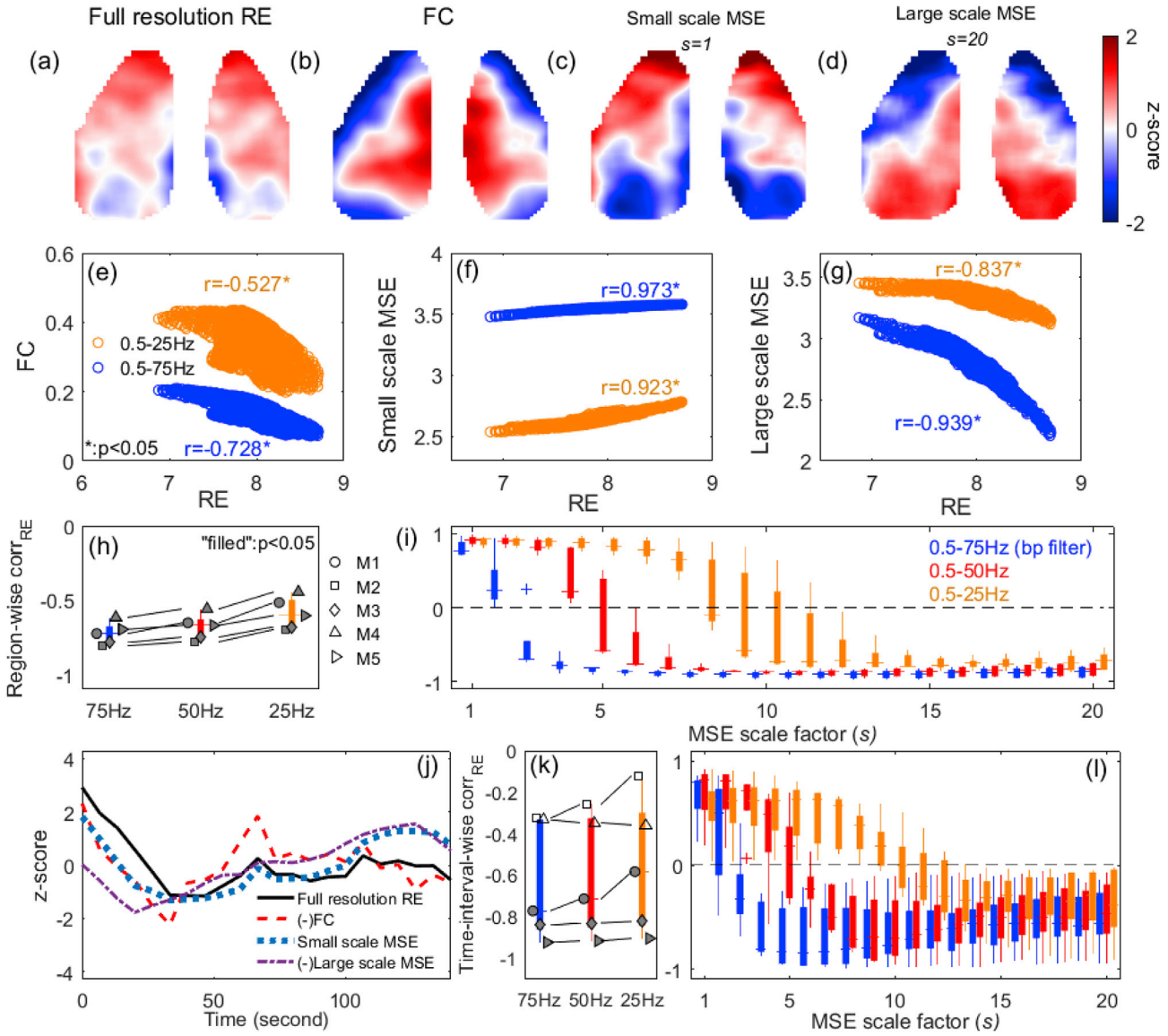

Fig. 6. RE-assessment by MSE and FC under temporal filtering of data. (a–d) Spatial maps of full resolution RE and recalculated FC, small scale MSE ($s = 1$) and large scale MSE ($s = 20$) from the full-length voltage signal in mouse #1 with 0.5–25 Hz bandpass filtering. (e–g) RE-FC (e), RE-small scale MSE (f), and RE-large scale MSE (g) correlations in mouse #1 with 0.5–25 Hz bandpass filtering (orange) and full resolution (blue, 0.5–75 Hz). (h) Region-wise RE-FC correlation changes with increasing temporal filtering (cut-off frequency from 75 Hz in full resolution data to 25 Hz). (i) Region-wise RE-MSE correlations across scale factors under temporal filtering. P-values for (h) and (i) under the same filtering were corrected together. (j) The time evolution of the global mean value of full resolution RE and FC, small scale MSE and large scale MSE from mouse #1 under 0.5–25 Hz bandpass filtering. (k)–(l) The plots corresponding to (h) and (i), but here calculated from time evolution in (j). P-values in (k) and (l) under the same filtering were corrected together. Scatter plots for individual mice for (i) and (l) are shown in Fig. A9.

3.4.2. Hemodynamics effects on the performance of FC in assessing RE

To simulate FC measures derived from fMRI data, we converted our voltage signal into simulated BOLD signal by applying a response function that implements temporal averaging and a delay as described in combined electrophysiological fMRI experiments (Logothetis et al., 2001, Fig. 7, see Methods). The simulated BOLD signal exhibited slow fluctuations and a frequency power spectrum that peaked near 0.09 Hz in contrast to the optical voltage signal that had peak power frequency at 1.94 Hz (Fig. 7 (b), (d)). We also simulated the typically slow sampling rate used in fMRI by down-sampling the simulated BOLD signal to 1 Hz. Unfortunately, the short length of the resulting time series (148 time points), similar to typical fMRI time series length, is not sufficient for MSE to reliably reflect the underlying signal variability, in particular when coarse-graining at large scales. Therefore, we explored the FC-RE correlation rather than MSE-RE correlation under this condition.

In Fig. 7 (f), the recalculated FC map exhibited patterns that clearly different from the full resolution RE and previous FC maps. For mouse #1, the new FC-RE correlation exhibited high non-linearity ($r = -0.553$, $p < 0.001$, Fig. 7 (g)), similar to observations under temporal filtering (Fig. 6 (e)). In the remaining 4 mice, different levels of increasing exhibited in the FC-RE correlation, leading to positive correlations in 3 mice (Fig. 7 (h)). When exploring the FC-RE correlation in time, it can be observed that the FC fluctuation in BOLD activity displayed a similar trend as the RE variation (Fig. 7 (i)). In the whole dataset, the FC-RE correlations in 4 mice moved closer to zero but maintained negative, 1 of which appeared to be significant under both optical voltage and BOLD signals (Fig. 7 (j)).

3.4.3. Spatial smoothing effects on the performance of MSE and FC in assessing RE

Finally, we reduced the spatial resolution of our voltage imaging data to compare with EEG conditions using Gaussian spatial smoothing with different kernel standard deviations σ (1 and 3, corresponding to smoothing window size of 5 and 13 pixels, i.e. 330 μm and 858 μm of cortical tissue). The resulting spatial patterns of FC and MSE seemed also to be smoothened (Fig. 8 (b)-(d)), and the RE-FC and RE-MSE

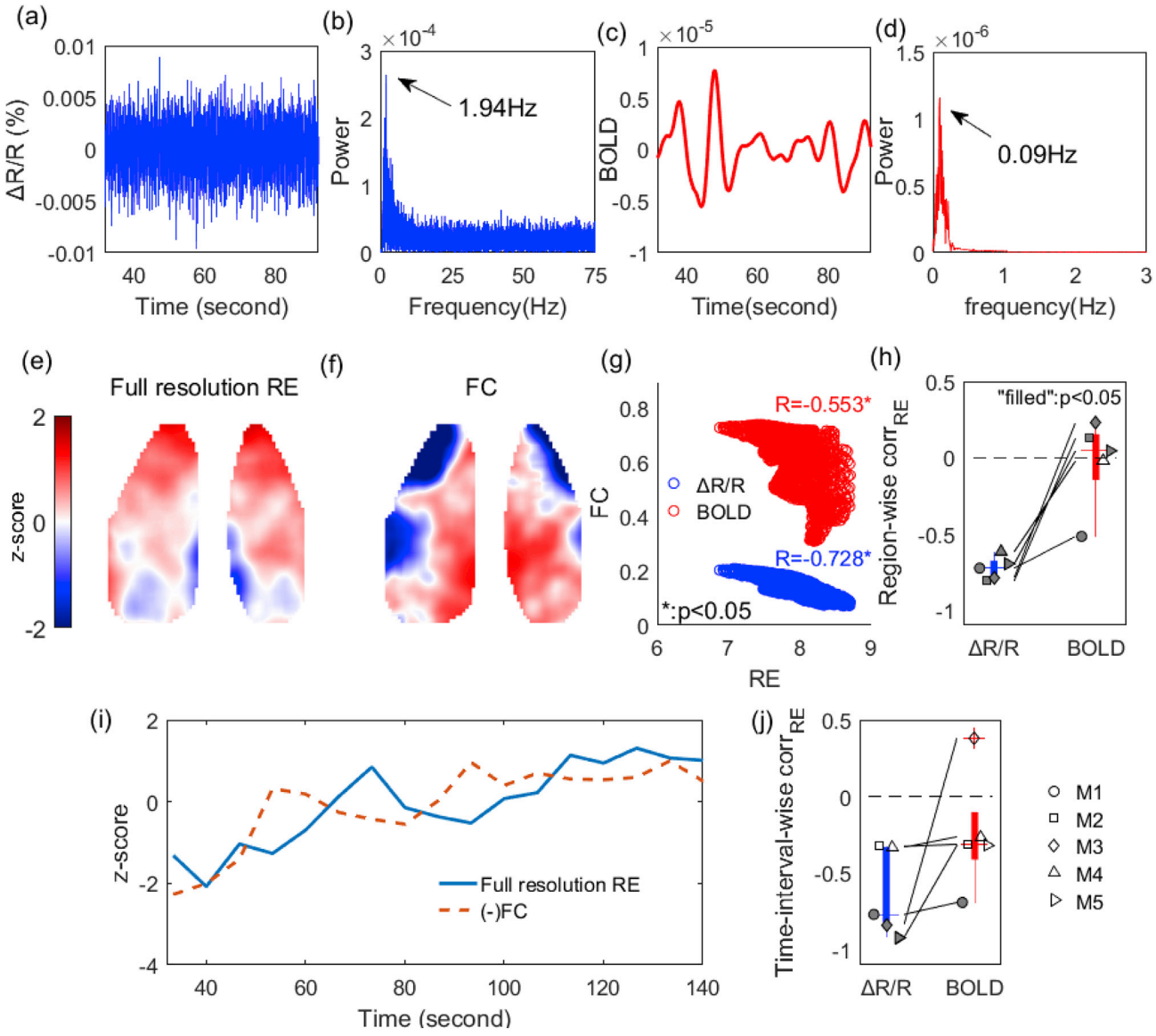

Fig. 7. RE-assessment by FC in simulated BOLD signal. (a–b) An example trace of the original optical voltage signal (a) and its corresponding power spectrum (b). (c) The simulated BOLD signal using (a) before down-sampling to 1 Hz. (d) The power spectrum of simulated BOLD signal in (c). (e)–(f) map of the full resolution RE and recalculated FC from mouse #1. (g) RE-FC using original signal and the simulated BOLD signal. (h) The original and recalculated region-wise FC-RE correlations across cortical space. (i) The time evolution of the global mean value of full resolution RE and recalculated FC from mouse #1. (Note the onset now at 32 s that due to the hemodynamics response function; see Methods.) (j) The corresponding plot of (h) but from time evolution in (i).

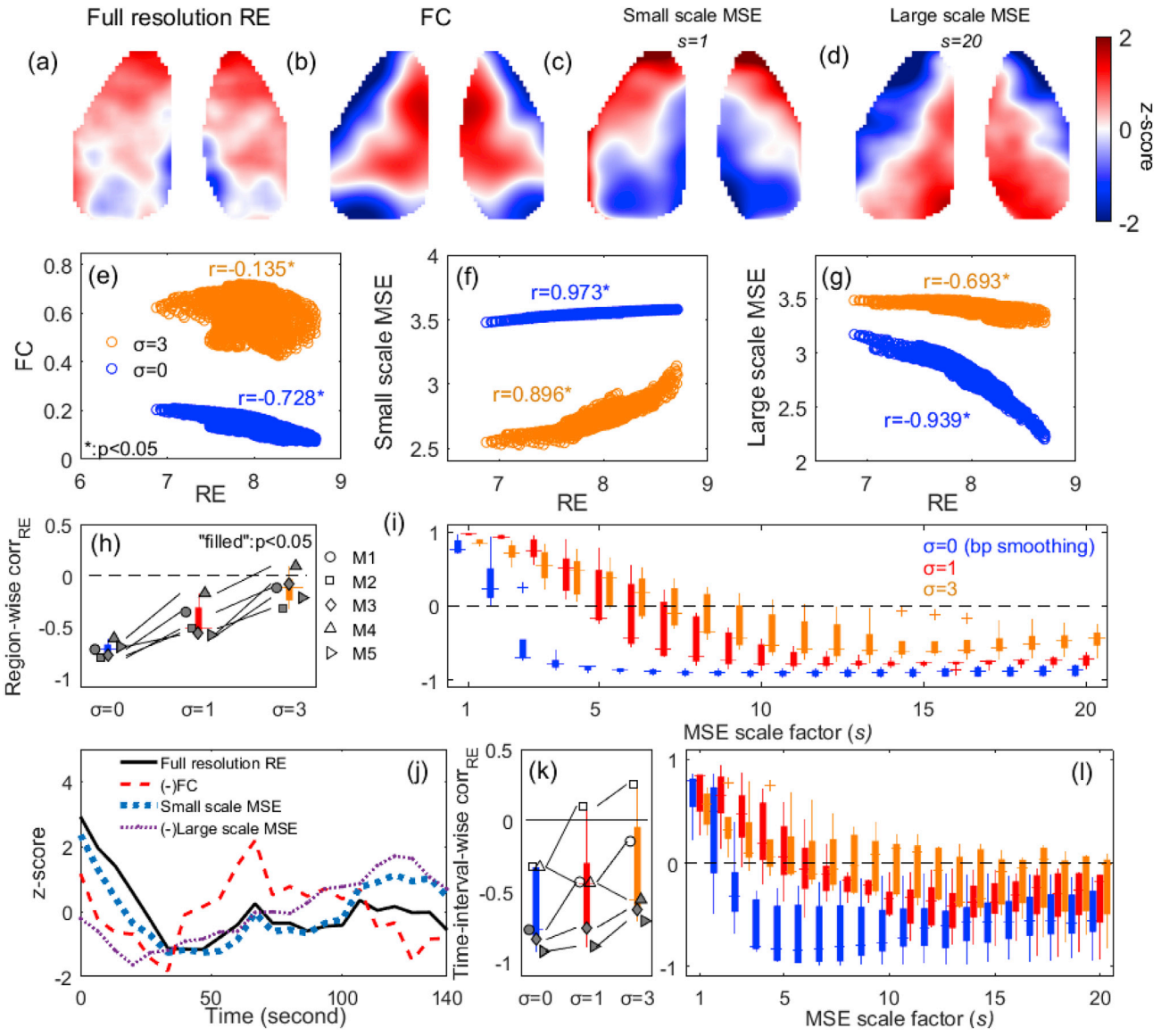

Fig. 8. RE-assessment by MSE and FC using spatially smoothed data. (a)–(d) Spatial maps of the full resolution RE, FC, small scale MSE and large scale MSE recalculated after spatial smoothing (Gaussian kernel, $\sigma = 3$). Mouse #1. (e)–(g) RE-FC (e), RE-small scale MSE (f), and RE-large scale MSE (g) with (orange; $\sigma = 3$) and without (blue, full resolution, $\sigma = 0$) spatial smoothing. Mouse #1. (h) Group level region-wise RE-FC correlation at different levels of spatial smoothing. (i) Region-wise RE-MSE correlation across scale with different levels of spatial smoothing. P-values for (h) and (i) under the same smoothing were corrected together. (j) The time evolution of the global mean value of full resolution RE, FC, small scale MSE, and large scale MSE from Mouse #1 with $\sigma = 3$ spatial smoothing. (k)–(l) Plots of time-interval-wise correlations; otherwise as in (h) and (i). The individual scatters for correlation and p-values of (i) and (l) are shown in Fig. A9.

correlations appear to lose their linear relationship after resolution reduction. (Fig. 8 (e)-(g)). As a result, the strength of FC-RE correlation approached zero or became positive (Fig. 8 (h)). The MSE-RE correlation still decreased with increasing MSE scale factors, although the zero-transition was shifted towards larger scales with spatial data smoothing (Fig. 8 (i)). While the absolute correlation values were weakened across all MSE scales, statistically significant correlations were kept at small and large scales even with the strongest spatial smoothing (Fig. 8 (i) and Fig. A9).

In the time domain, with strong spatial smoothing, the FC changes are more de-coupled from RE in the example mouse (Fig. 8 (j), red). However, across animals the effect of smoothing was not consistent. The decoupling between FC and RE holds for four out of five mice for the two investigated smoothing strengths (Fig. 8 (k)), while for the remaining one, FC-RE correlation was enhanced. At the same time, strong smoothing diminished the MSE-RE correlations strength at high scales. When $\sigma = 3$, the box plots overlapped with the zero line starting from scale 4 (Fig. 8 (l)), which indicates the non-significance of the correlations in individuals (Fig. A9).

4. Discussion

Voltage imaging of the mouse cortex at high spatiotemporal resolution provides rich information on neuronal dynamics in space and time. In this work, we took this opportunity to systematically examine the capability of temporal variability measure (Multiscale Entropy; MSE) and spatiotemporal synchronization measure (Functional Connectivity; FC) in assessing the spatiotemporal variability (Regional Entropy; RE) across the mouse dorsal cortex, their temporal evolution, and brain state dependency. We observed a strong negative linear correlation between FC and RE across cortical space and temporal evolution (Fig. 3). MSE and RE correlated positively in small scales and negatively in large scales. Larger temporal scales ($s > 10$) reduced MSE-RE correlation towards non-significant values in 2/5 mice. These correlations were preserved when the brain state was altered by an anesthetic agent (Fig. 4). The observed correlations resulted in the coupling between the MSE and FC measures in individuals and groups (Fig. 5). We further explored if our results may hold under the conditions of human neuroimaging modalities using temporal/spatial smoothing and a model for converting electrical neuronal population activity into BOLD signals (Figs. 6–8). This exploration suggested that, although affected by the reduced resolutions, FC and MSE can still partially provide assessments of the structural and dynamics variation of the original high-resolution RE.

Strong synchrony limits the repertoire of activity patterns generated by neuronal circuits while weak spatial coupling allows the emergence of more diverse patterns in space. This explains the negative FC-RE relationship. The scale-dependent MSE-RE correlations are in line with insights from previous studies showing that small scale MSE is related to local information processing, described by RE here, and large scale MSE associates with long range communications (Vakorin et al., 2011; McIntosh et al., 2014). In addition, model-based and empirical studies indicated that small scale MSE contains information about the higher frequency components of neuronal activity while large scale MSE tends to relate to slow neuronal oscillations (Courtiol et al., 2016; Lippe et al., 2009; McIntosh et al., 2014). Therefore, small and large scale MSE inform on different neurophysiological mechanisms. The correlation between FC/MSE and RE in space and time leads to a corresponding co-variation of these measures when comparing individual subjects and groups. Anesthesia reduced RE, strengthened FC and decreased/increased MSE at small/large scales respectively, and thus FC was negatively/positively correlated to MSE at small/large scales. This finding is consistent with previous sleep studies using human neuroimaging, where FC calculated from fMRI data increased within the dorsal attention network during light sleep (Larson-Prior et al., 2009), while MSE in EEG globally decreased/increased at small/large scales respectively during deep sleep (Shi et al., 2017; Miskovic et al., 2018). Another example where the relationship between FC and MSE has been indirectly indicated is during the process of normal aging. With increasing age, resting state fMRI FC reduced in large parts of the brain (Dennis and Thompson, 2014; Ferreira and Busatto, 2013), which associates with observed MSE increase/decrease at small/large scales in EEG (Vakorin et al., 2011; McIntosh et al., 2014), consistent with the relationships described here. Taken together, insights from the present work helps to reconcile the different analysis approaches applied in human sleep and aging studies. Although we only explored brain state dependency of our measures for the case of anesthesia, we would expect that other brain state modifications would be similarly reflected by analysis of voltage imaging data obtained from appropriate mouse models.

We then explored the relevance of our findings based on high resolution voltage imaging to human neuroimaging modalities. During the spatiotemporal smoothing tests, we found both FC-RE and MSE-RE correlations in space and time could largely maintain unless the spatiotemporal information was severely destroyed. FC-RE correlations across cortical seed regions were strongly affected by application of the linear hemodynamics response function (simulating BOLD signals), but the time-interval-wise associations were largely preserved. This gave confidence that FC and MSE are capable of capturing information related to RE using human neuroimaging technology associated with reduced spatiotemporal resolution.

In this analysis, the effect of sampling rate on the MSE-RE correlation was not explicitly considered. The scale factors in MSE need to be interpreted relative to the sampling rate and the frequency spectrum of the biological signals, and thus our results can be applied to human studies using different acquisition rates/down sampling schemes by matching the scale expressed in physical time units. Interestingly, we observed that the positive-to-negative transition in MSE-RE correlation along scales could be influenced by the change of spatial and temporal smoothing. However, here the MSE-RE correlation change was demonstrated under the same sampling rate and only the frequency spectrum of the signal was varied. This suggested that the interpretation of MSE at different scales should also be associated to the captured spatiotemporal frequency bandwidth of the signals, which was clearly demonstrated and explained in Courtiol et al. (2016). This dependency of MSE scale on captured frequency complicates the cross comparison among MSE studies under different filtering schemes and data modalities. A measure integrating information cross scales could be plausible to avoid this difficulty, such as the scaling of MSE decay along scales (Gao et al., 2015; Takahashi et al., 2009; Courtiol et al., 2016), which could extract information about scale-free property, i.e. self-similarity in the signal under proper assumption (Gao et al., 2015).

In conclusion, the present work may help with the interpretation of two biomarkers (FC and MSE) and provided a promising framework for integration of the knowledge obtained from divergent imaging modalities (EEG and fMRI).

Acknowledgements

This work was supported by Hong Kong Baptist University (HKBU) Strategic Development Fund, the Hong Kong Research Grant Council (GRF12200217), and HKBU FRG2/17-18/011, and HKBU Interdisciplinary Research Matching Scheme (IRMS/16-17/04) to CSZ and the National Institutes of Health BRAIN initiative grant 1U01MH109091 to TK. The authors declare no conflict of interest.

Appendix

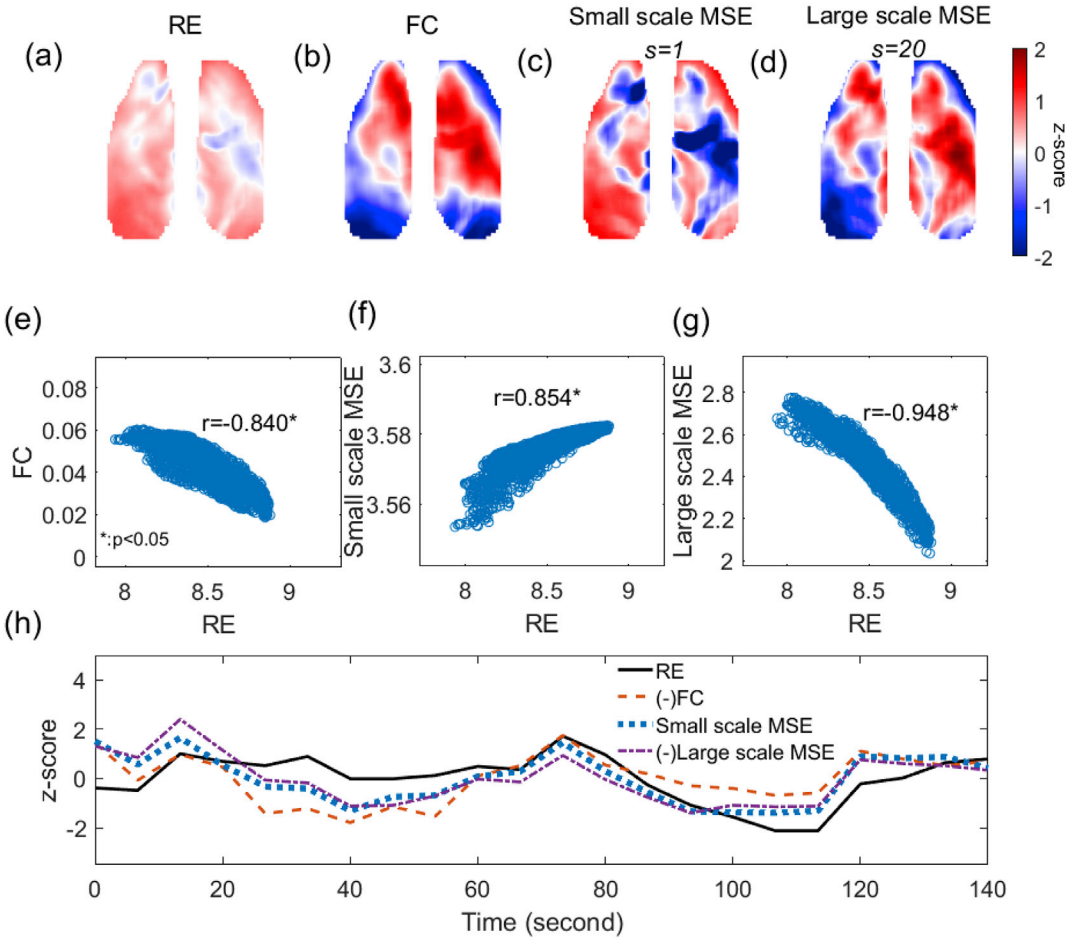

Fig. A1. related to Fig. 3. MSE, FC, RE spatial and temporal patterns and their correlations for Mouse #2 under wakefulness with 0.5–75Hz filter. (a)–(d) Spatial patterns for (a) RE, (b) FC, (c) small scale MSE ($s = 1$) and (d) large scale MSE ($s = 20$). (e-g) Cortex-wide region-wise correlation of (e) RE-FC, (f) RE-small scale MSE, and (g) RE-large scale MSE using data from (a-d). (h) Z-score showing the temporal evolution of the spatial average across all seed regions for RE, FC, small scale MSE and large scale MSE for Mouse #2.

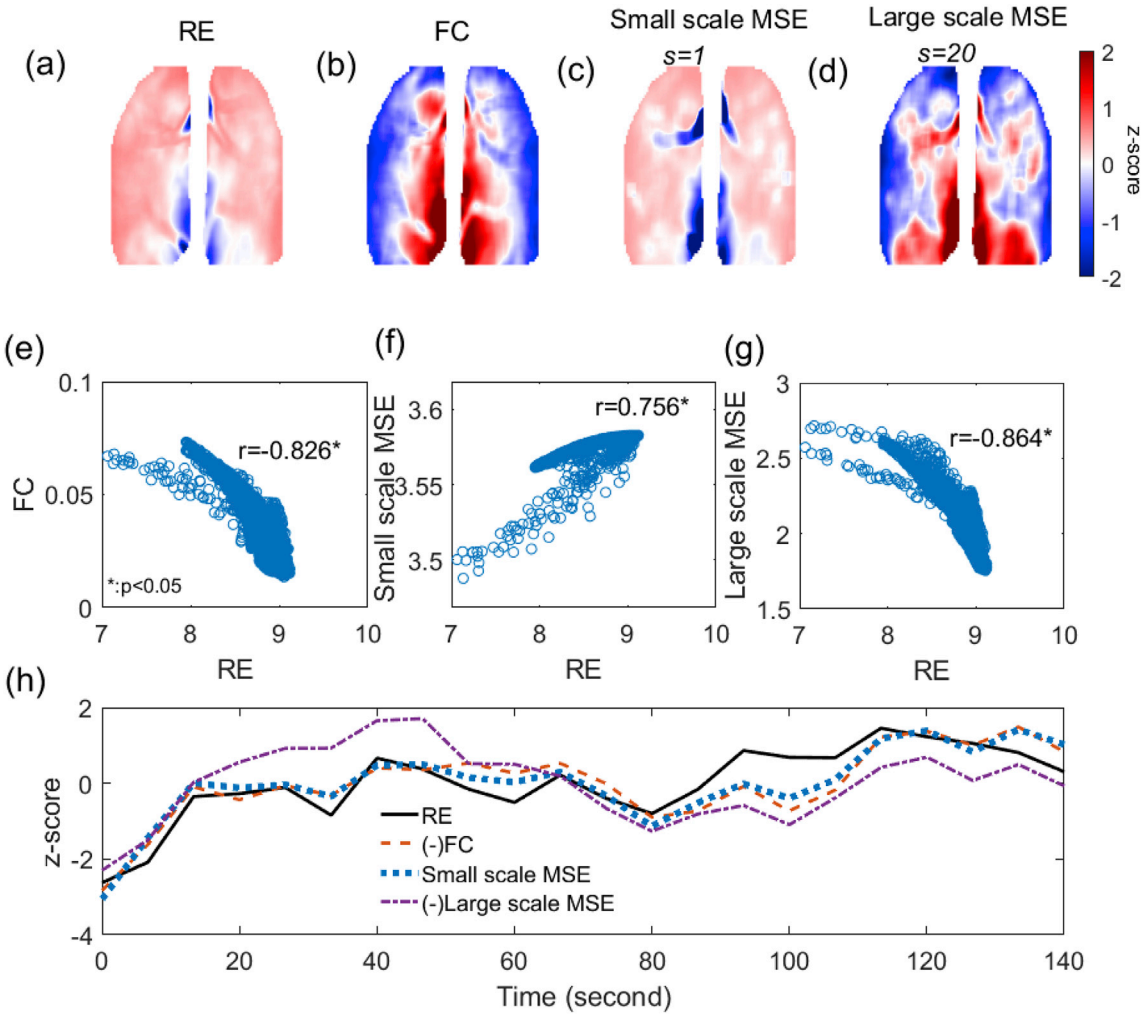

Fig. A2. related to Fig. 3. Individual result for mouse #3 under wakefulness using 0.5Hz high-pass filter. Same layout as Fig. A1.

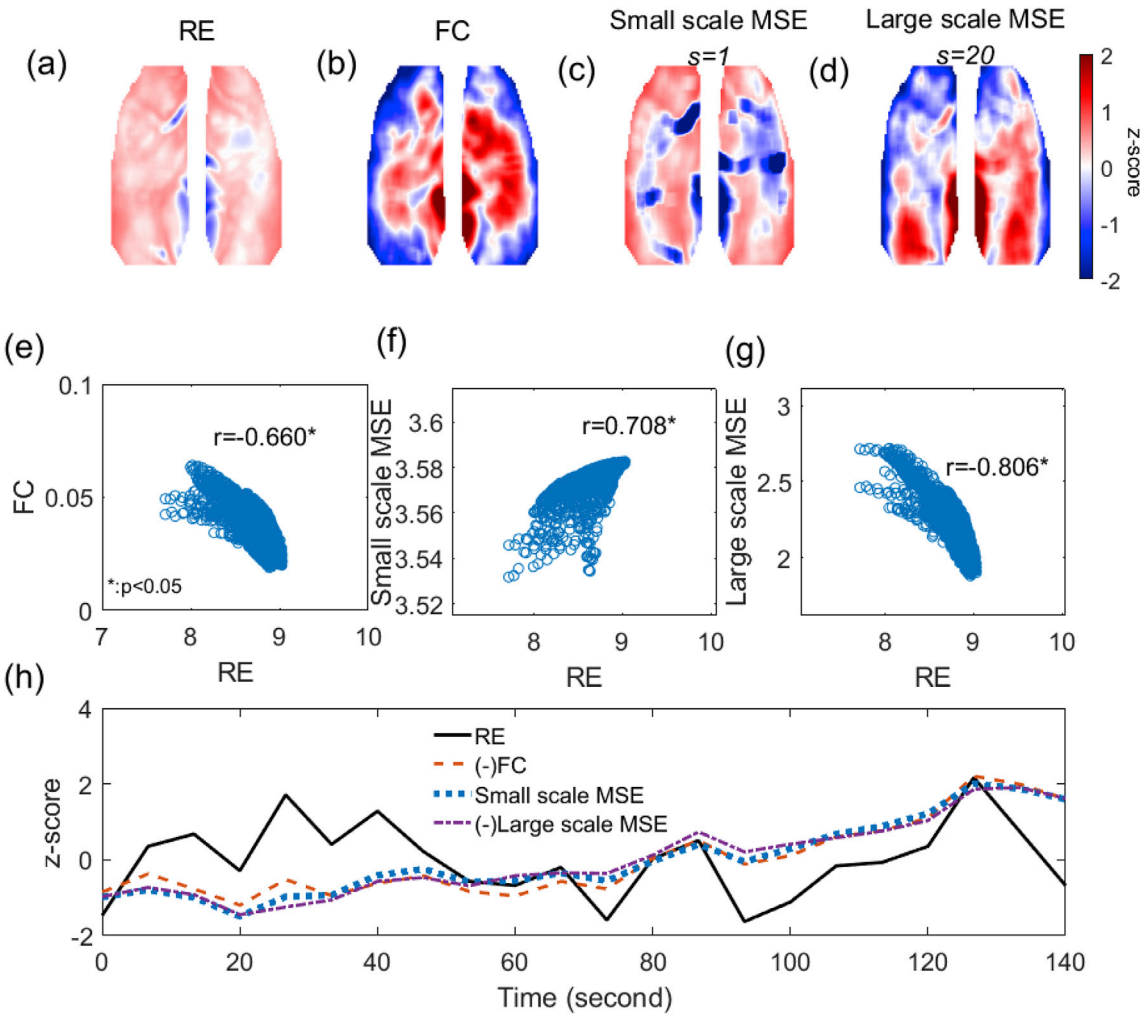

Fig. A3. related to Fig. 3. Individual result for mouse #4 under wakefulness using 0.5Hz high-pass filter. Same layout as Fig. A1.

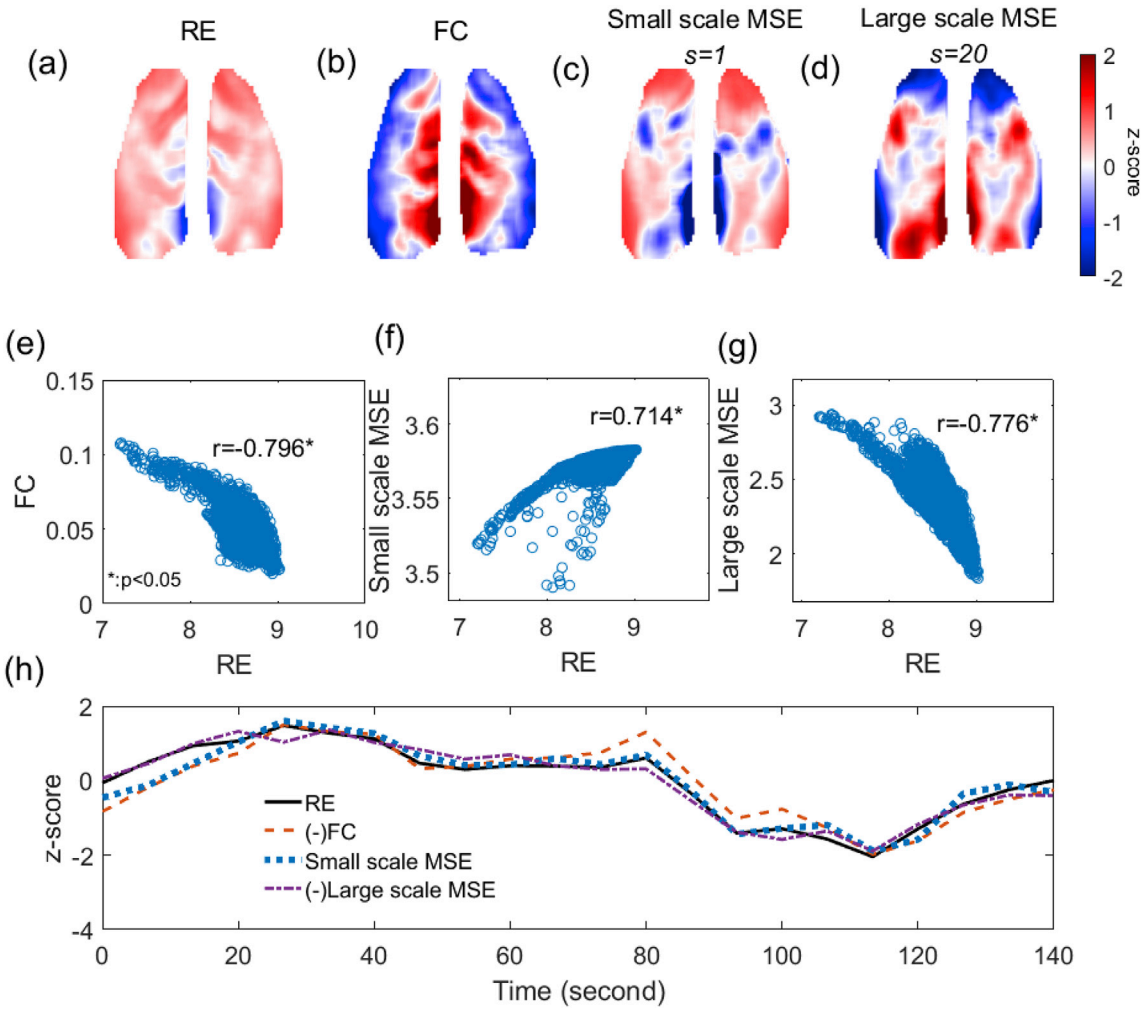

Fig. A4. related to Fig. 3. Individual result for mouse #5 under wakefulness using 0.5Hz high-pass filter. Same layout as Fig. A1.

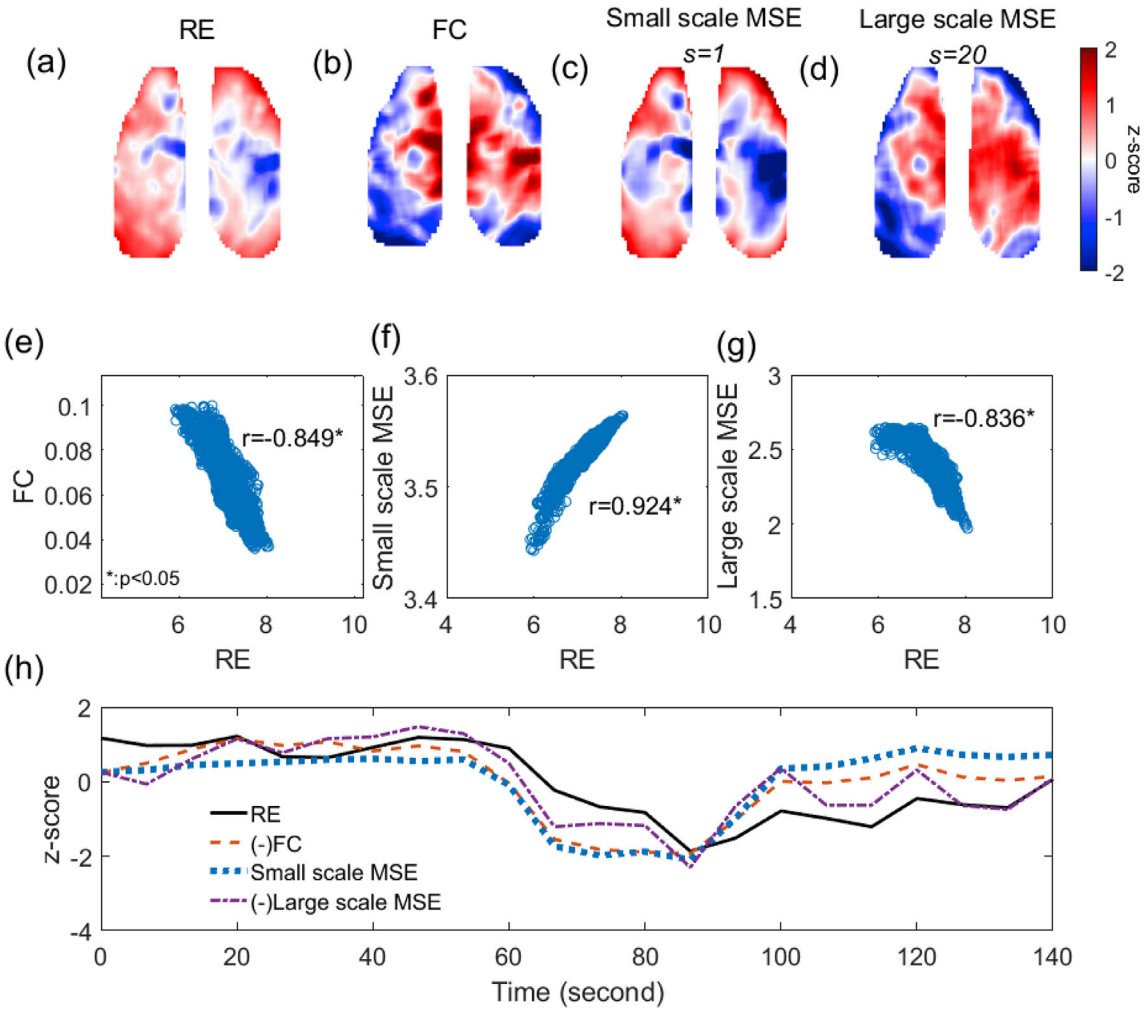

Fig. A5. related to Fig. 4. Individual result for mouse #2 under anesthesia using 0.5Hz high-pass filter. Same layout as Fig. A1.

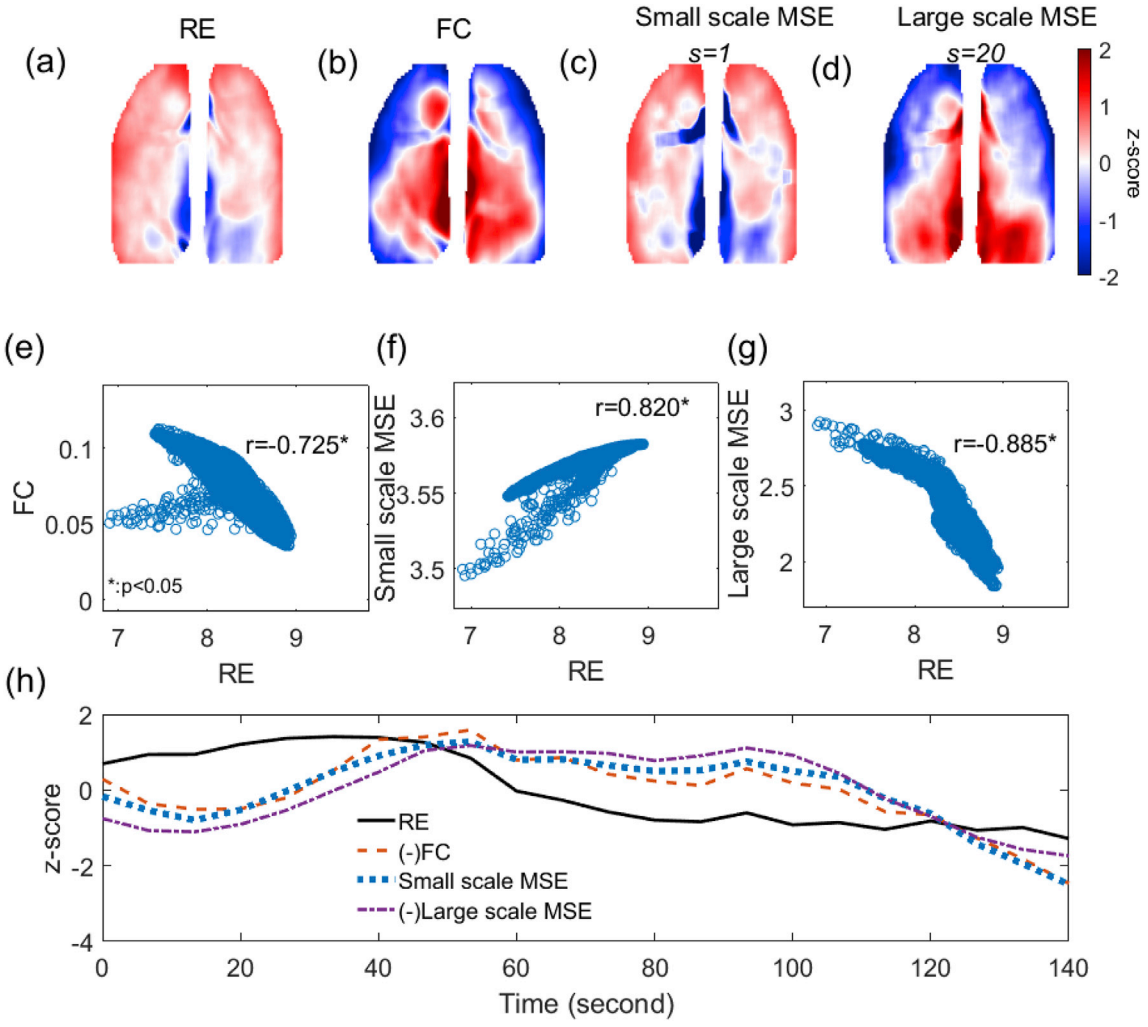

Fig. A6. related to Fig. 4. Individual result for mouse #3 under anesthesia using 0.5Hz high-pass filter. Same layout as Fig. A1.

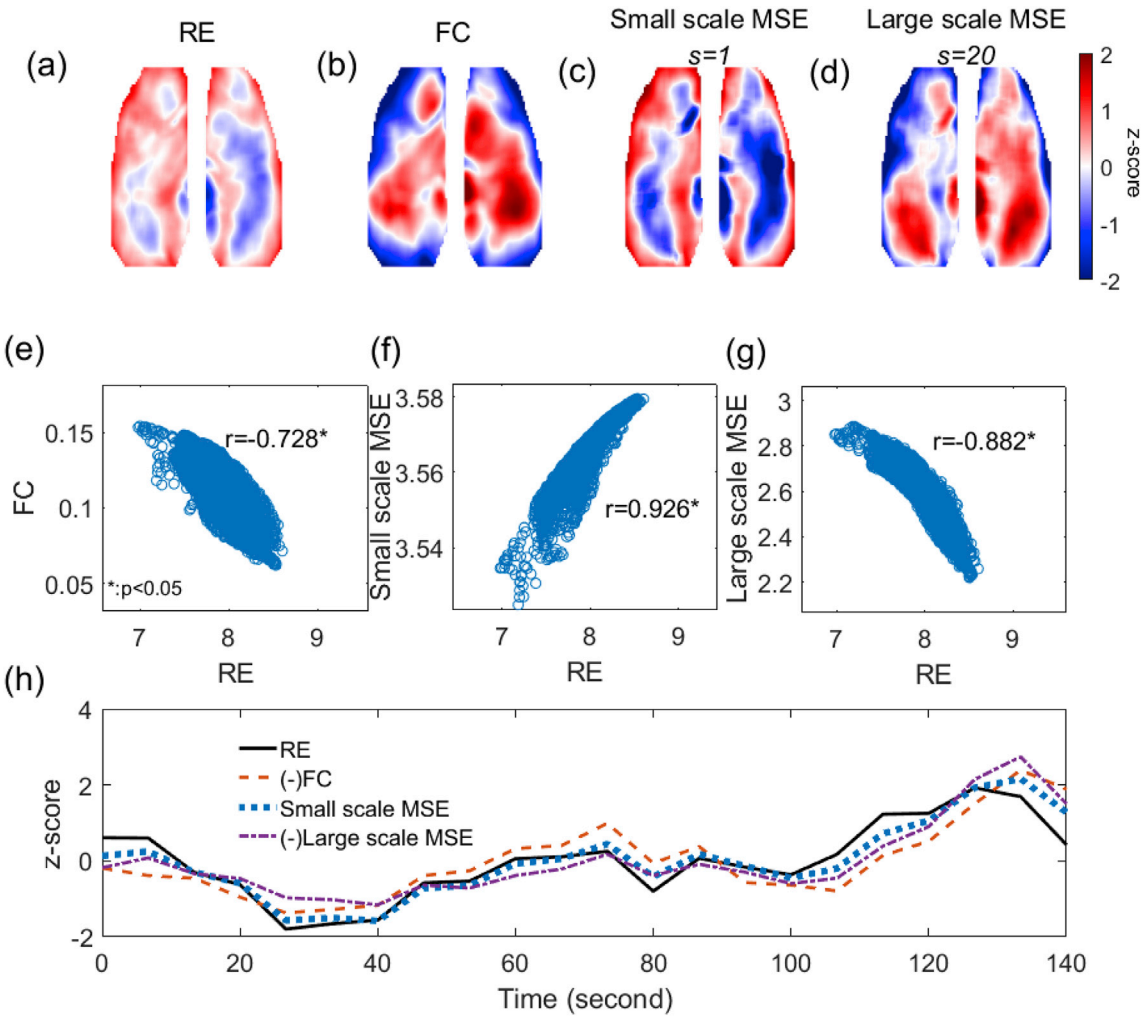

Fig. A7. related to Fig. 4. Individual result for mouse #4 under anesthesia using 0.5Hz high-pass filter. Same layout as Fig. A1.

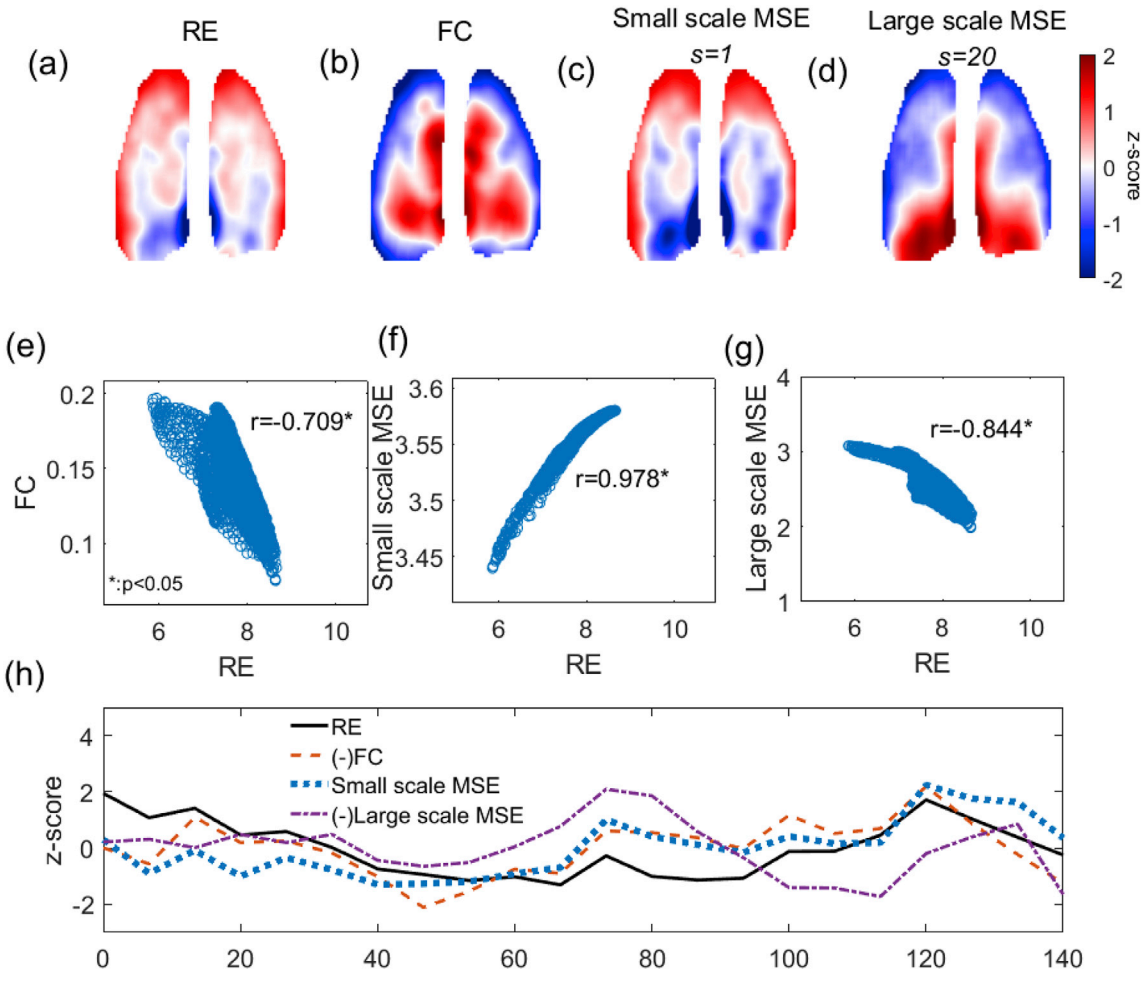

Fig. A8. related to Fig. 4. Individual result for mouse #5 under anesthesia using 0.5Hz high-pass filter. Same layout as Fig. A1.

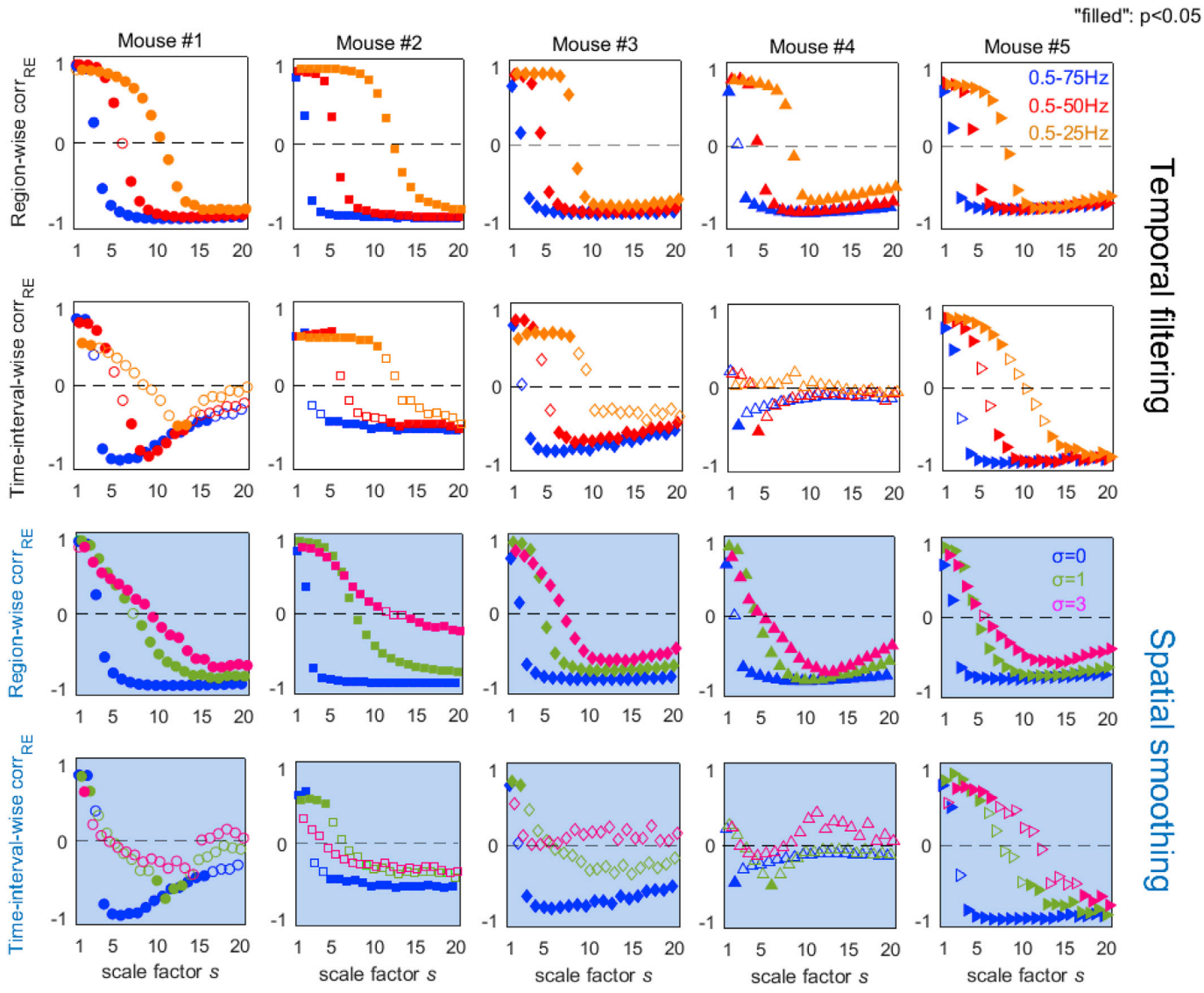

Fig. A9. related to Figs. 6 and 8. Changes of MSE-RE correlation under different temporal filtering and spatial smoothing for individual mice under wakefulness condition. (a-b) Cortex-wide region-wise (a) and time-interval-wise (b) RE-MSE correlations across scale factors under different temporal filtering. (c-d) Cortex-wide region-wise (c) and time-interval-wise (d) RE-MSE correlations across scale factors under different spatial smoothing.

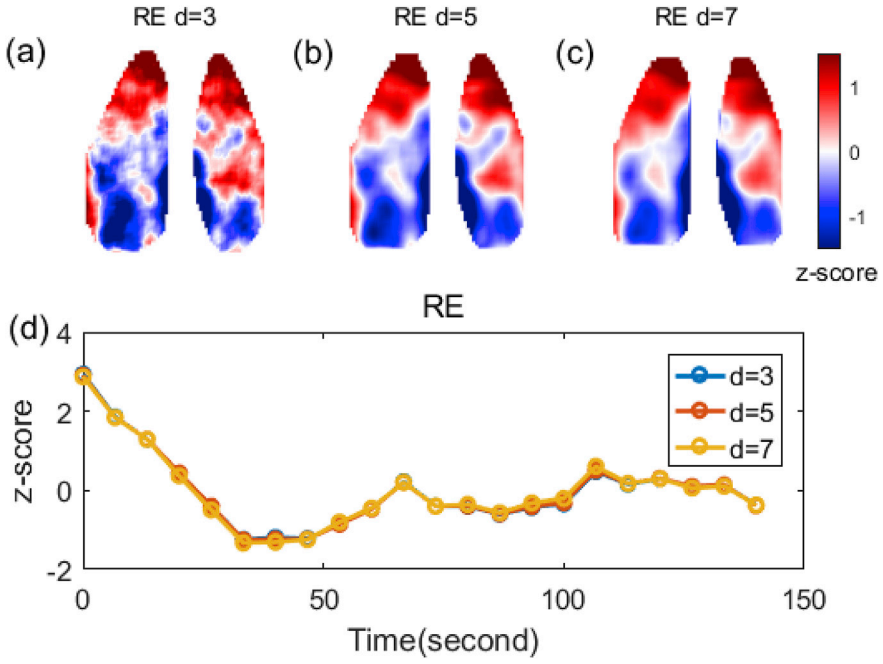

Fig. A10. additional analysis. Effects of seed region window size on RE calculations. (a)–(c) Spatial maps of RE from square seed regions with window sizes of $d = 3$, 5, 7 pixels. (d) Time series of cortex-wide averaged RE with spatial window sizes of $d = 3$, 5, 7 pixels.

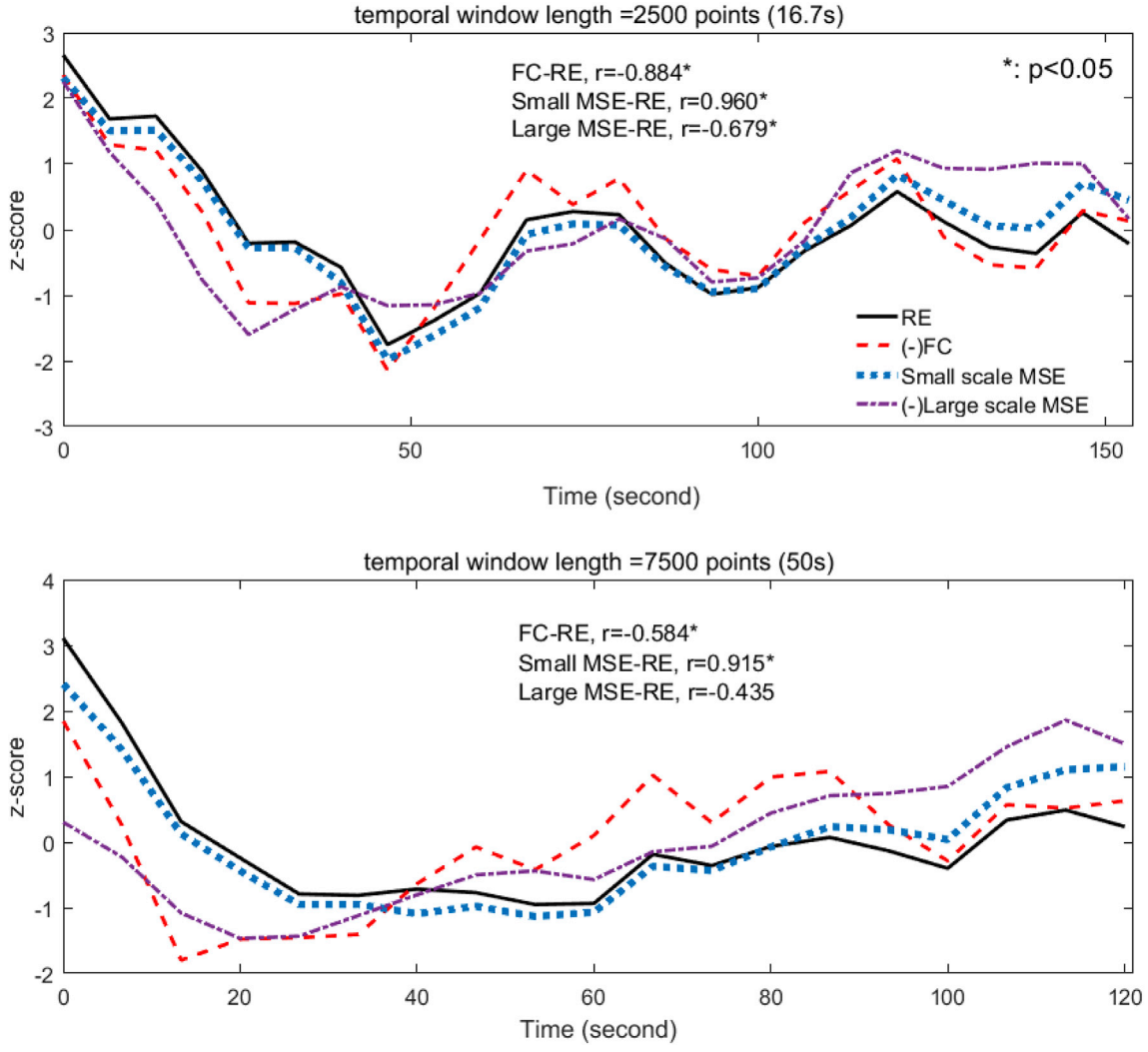

Fig. A11. additional analysis. Effects of sliding window size on the measuring time evolution of cortex-wide averaged RE, MSE and FC. Time evolution of cortical means of RE, FC and MSE with temporal window length 16.7 s (top) and 50 s (bottom).

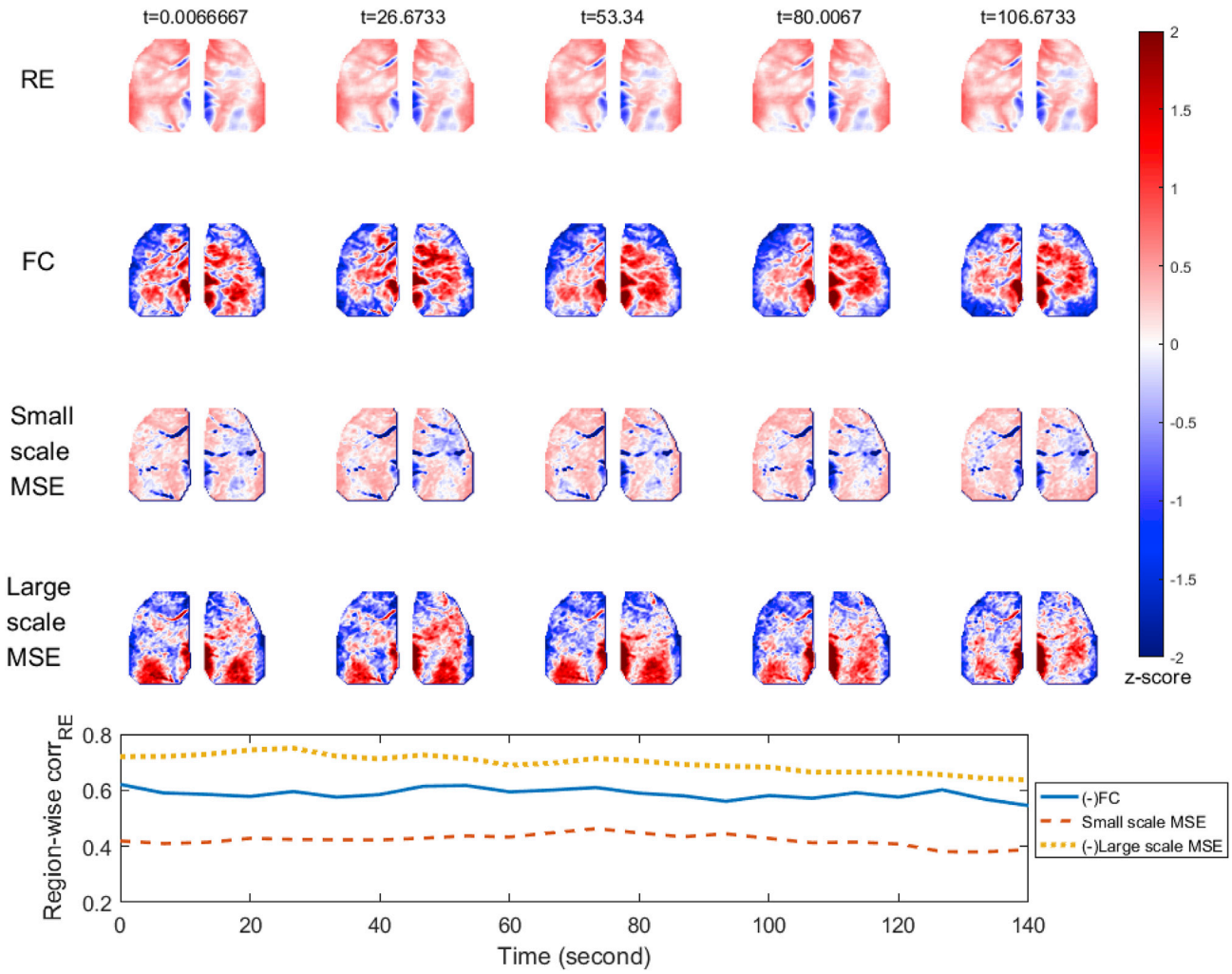

Fig. A12. additional analysis. Temporal changes of region-wide FC-RE and MSE-RE correlations from an example mouse (Mouse #3) under anesthesia condition. The spatial maps changes are given on the top and the estimated region-wise RE correlations from FC, small scale MSE ($s = 1$) and large scale MSE ($s = 20$) are plotted underneath. From Fig. A6figA6, it can be observed that time-interval-wide FC and MSE values did not co-varying with RE. However, the region-wide FC-RE and MSE-RE correlations remain almost constant in different temporal windows.

References

Akemann, W., Mutoh, H., Perron, A., Rossier, J., Knöpfel, T., 2010. Imaging brain electric signals with genetically targeted voltage-sensitive fluorescent proteins. Nat. Methods 7, 643.

Akemann, W., Mutoh, H., Perron, A., Park, Y.K., Iwamoto, Y., Knöpfel, T., 2012. Imaging neural circuit dynamics with a voltage-sensitive fluorescent protein. J. Neurophysiol. 108, 2323–2337.

Akemann, W., Sasaki, M., Mutoh, H., Imamura, T., Honkura, N., Knöpfel, T., 2013. Two-photon voltage imaging using a genetically encoded voltage indicator. Sci. Rep. 3, 2231.

Assaf, M., Jagannathan, K., Calhoun, V.D., Miller, L., Stevens, M.C., Sahl, R., et al., 2010. Abnormal functional connectivity of default mode sub-networks in autism spectrum disorder patients. Neuroimage 53, 247–256.

Avena-Koenigsberger, A., Misic, B., Sporns, O., 2018. Communication dynamics in complex brain networks. Nat. Rev. Neurosci. 19, 17.

Azami, H., Rostaghi, M., Abásolo, D., Escudero, J., 2017. Refined composite multiscale dispersion entropy and its application to biomedical signals. IEEE Trans. Biomed. Eng. 64, 2872–2879.

Bak, P., Tang, C., Wiesenfeld, K., 1987. Self-organized criticality: an explanation of the 1/f noise. Phys. Rev. Lett. 59, 381.

Bandettini, P.A., 2014. Neuronal or hemodynamic? Grappling with the functional MRI signal. Brain Connect. 4, 487–498.

Beharelle, A.R., Kovačević, N., McIntosh, A.R., Levine, B., 2012. Brain signal variability relates to stability of behavior after recovery from diffuse brain injury. Neuroimage 60, 1528–1537.

Bosl, W., Tierney, A., Tager-Flusberg, H., Nelson, C., 2011. EEG complexity as a biomarker for autism spectrum disorder risk. BMC Med. 9, 18.

Catarino, A., Churches, O., Baron-Cohen, S., Andrade, A., Ring, H., 2011. Atypical EEG complexity in autism spectrum conditions: a multiscale entropy analysis. Clin. Neurophysiol. 122, 2375–2383.

Cocchi, L., Gollo, L.L., Zalesky, A., Breakspear, M., 2017. Criticality in the brain: a synthesis of neurobiology, models and cognition. Prog. Neurobiol. 158, 132–152.

Costa, M., Goldberger, A.L., Peng, C.K., 2002. Multiscale entropy analysis of complex physiologic time series. Phys. Rev. Lett. 89, 068102.

Costa, M., Peng, C.K., Goldberger, A.L., Hausdorff, J.M., 2003. Multiscale entropy analysis of human gait dynamics. Phys. Stat. Mech. Appl. 330, 53–60.

Courtiol, J., Perdikis, D., Petkoski, S., Müller, V., Huys, R., Sleimen-Malkoun, R., Jirsa, V.K., 2016. The multiscale entropy: guidelines for use and interpretation in brain signal analysis. J. Neurosci. Methods 273, 175–190.

Dennis, E.L., Thompson, P.M., 2014. Functional brain connectivity using fMRI in aging and Alzheimer's disease. Neuropsychol. Rev. 24, 49–62.

Escudero, J., Abásolo, D., Hornero, R., Espino, P., López, M., 2006. Analysis of electroencephalograms in Alzheimer's disease patients with multiscale entropy. Physiol. Meas. 27, 1091.

Fagerholm, E.D., Scott, G., Shew, W.L., Song, C., Leech, R., Knöpfel, T., Sharp, D.J., 2016. Cortical entropy, mutual information and scale-free dynamics in waking mice. Cerebr. Cortex 26, 3945–3952.

Faisal, A.A., Selen, L.P., Wolpert, D.M., 2008. Noise in the nervous system. Nat. Rev. Neurosci. 9, 292.

Ferreira, L.K., Busatto, G.F., 2013. Resting-state functional connectivity in normal brain aging. Neurosci. Biobehav. Rev. 37, 384–400.

Fornito, A., Zalesky, A., Breakspear, M., 2015. The connectomics of brain disorders. Nat. Rev. Neurosci. 16, 159.

Gao, J., Hu, J., Liu, F., Cao, Y., 2015. Multiscale entropy analysis of biological signals: a fundamental bi-scaling law. Front. Comput. Neurosci. 9, 64.

Garrett, D.D., Samanez-Larkin, G.R., MacDonald, S.W., Lindenberger, U., McIntosh, A.R., Grady, C.L., 2013. Moment-to-moment brain signal variability: a next frontier in human brain mapping? Neurosci. Biobehav. Rev. 37, 610–624.
Ghanbari, Y., Bloy, L., Edgar, J.C., Blaskey, L., Verma, R., Roberts, T.P., 2015. Joint analysis of band-specific functional connectivity and signal complexity in autism. J. Autism Dev. Disord. 45, 444–460.
Grandy, T.H., Garrett, D.D., Schmiedek, F., Werkle-Bergner, M., 2016. On the estimation of brain signal entropy from sparse neuroimaging data. Sci. Rep. 6, 23073.
Heisz, J.J., Shedden, J.M., McIntosh, A.R., 2012. Relating brain signal variability to knowledge representation. Neuroimage 63, 1384–1392.
Keller, D., Erö, C., Markram, H., 2018. Cell densities in the mouse brain: a systematic review. Front. Neuroanat. 12.
Kuntzelman, K., Miskovic, V., 2017. Reliability of graph metrics derived from resting-state human EEG. Psychophysiology 54, 51–61.
Kuntzelman, K., Rhodes, L.J., Harrington, L.N., Miskovic, V., 2018. A practical comparison of algorithms for the measurement of multiscale entropy in neural time series data. Brain Cogn. 123, 126–135.
Larson-Prior, L.J., Zempel, J.M., Nolan, T.S., Prior, F.W., Snyder, A.Z., Raichle, M.E., 2009. Cortical network functional connectivity in the descent to sleep. Proc. Natl. Acad. Sci. U.S.A. 106, 4489–4494.
Lecci, S., Fernandez, L.M., Weber, F.D., Cardis, R., Chatton, J.Y., Born, J., Lüthi, A., 2017. Coordinated infraslow neural and cardiac oscillations mark fragility and offline periods in mammalian sleep. Sci. Adv. 3, e1602026.
Li, D., Li, X., Liang, Z., Voss, L.J., Sleigh, J.W., 2010. Multiscale permutation entropy analysis of EEG recordings during sevoflurane anesthesia. J. Neural Eng. 7, 046010.
Lippe, S., Kovacevic, N., McIntosh, A.R., 2009. Differential maturation of brain signal complexity in the human auditory and visual system. Front. Hum. Neurosci. 3, 48.
Logothetis, N.K., Pauls, J., Augath, M., Trinath, T., Oeltermann, A., 2001. Neurophysiological investigation of the basis of the fMRI signal. Nature 412, 150.
Lynall, M.E., Bassett, D.S., Kerwin, R., McKenna, P.J., Kitzbichler, M., Muller, U., Bullmore, E., 2010. Functional connectivity and brain networks in schizophrenia. J. Neurosci. 30, 9477–9487.
Mashour, G.A., Hudetz, A.G., 2018. Neural correlates of unconsciousness in large-scale brain networks. Trends Neurosci. 41, 150–160.
McDonough, I.M., Nashiro, K., 2014. Network complexity as a measure of information processing across resting-state networks: evidence from the Human Connectome Project. Front. Hum. Neurosci. 8, 409.
McIntosh, A.R., Kovacevic, N., Itier, R.J., 2008. Increased brain signal variability accompanies lower behavioral variability in development. PLoS Comput. Biol. 4, e1000106.
McIntosh, A.R., Vakorin, V., Kovacevic, N., Wang, H., Diaconescu, A., Protzner, A.B., 2014. Spatiotemporal dependency of age-related changes in brain signal variability. Cerebr. Cortex 24, 1806–1817.
Mishina, Y., Mutoh, H., Song, C., Knöpfel, T., 2014. Exploration of genetically encoded voltage indicators based on a chimeric voltage sensing domain. Front. Mol. Neurosci. 7, 78.
Miskovic, V., Keil, A., 2015. Reliability of event-related EEG functional connectivity during visual entrainment: magnitude squared coherence and phase synchrony estimates. Psychophysiology 52, 81–89.
Miskovic, V., MacDonald, K.J., Rhodes, L.J., Cote, K.A., 2018. Changes in EEG multiscale entropy and power-law frequency scaling during the human sleep cycle. Hum. Brain Mapp. 40, 538–551.
Mizuno, T., Takahashi, T., Cho, R.Y., Kikuchi, M., Murata, T., Takahashi, K., Wada, Y., 2010. Assessment of EEG dynamical complexity in Alzheimer's disease using multiscale entropy. Clin. Neurophysiol. 121, 1438–1446.
Mukamel, R., Gelbard, H., Arieli, A., Hasson, U., Fried, I., Malach, R., 2005. Coupling between neuronal firing, field potentials, and FMRI in human auditory cortex. Science 309, 951–954.
Mulders, P.C., van Eijndhoven, P.F., Schene, A.H., Beckmann, C.F., Tendolkar, I., 2015. Resting-state functional connectivity in major depressive disorder: a review. Neurosci. Biobehav. Rev. 56, 330–344.
Muller, L., Chavane, F., Reynolds, J., Sejnowski, T.J., 2018. Cortical travelling waves: mechanisms and computational principles. Nat. Rev. Neurosci. 19, 255.
Nir, Y., Fisch, L., Mukamel, R., Gelbard-Sagiv, H., Arieli, A., Fried, I., Malach, R., 2007. Coupling between neuronal firing rate, gamma LFP, and BOLD fMRI is related to interneuronal correlations. Curr. Biol. 17, 1275–1285.
Okazaki, R., Takahashi, T., Ueno, K., Takahashi, K., Higashima, M., Wada, Y., 2013. Effects of electroconvulsive therapy on neural complexity in patients with depression: report of three cases. J. Affect. Disord. 150, 389–392.
Palva, S., Palva, J.M., 2018. Roles of brain criticality and multiscale oscillations in temporal predictions for sensorimotor processing. Trends Neurosci. 41, 729–743.
Pincus, S.M., 1991. Approximate entropy as a measure of system complexity. Proc. Natl. Acad. Sci. U.S.A. 88, 2297–2301.
Privman, E., Nir, Y., Kramer, U., Kipervasser, S., Andelman, F., Neufeld, M.Y., et al., 2007. Enhanced category tuning revealed by intracranial electroencephalograms in high-order human visual areas. J. Neurosci. 27, 6234–6242.
Richman, J.S., Moorman, J.R., 2000. Physiological time-series analysis using approximate entropy and sample entropy. Am. J. Physiol. Heart Circ. Physiol. 278, H2039–H2049.
Rostaghi, M., Azami, H., 2016. Dispersion entropy: a measure for time-series analysis. IEEE Signal Process. Lett. 23, 610–614.
Sakkalis, V., 2011. Review of advanced techniques for the estimation of brain connectivity measured with EEG/MEG. Comput. Biol. Med. 41, 1110–1117.
Schoffelen, J.M., Gross, J., 2009. Source connectivity analysis with MEG and EEG. Hum. Brain Mapp. 30, 1857–1865.
Scott, G., Fagerholm, E.D., Mutoh, H., Leech, R., Sharp, D.J., Shew, W.L., Knöpfel, T., 2014. Voltage imaging of waking mouse cortex reveals emergence of critical neuronal dynamics. J. Neurosci. 34, 16611–16620.
Shew, W.L., Plenz, D., 2013. The functional benefits of criticality in the cortex. Neuroscientist 19, 88–100.
Shew, W.L., Yang, H., Petermann, T., Roy, R., Plenz, D., 2009. Neuronal avalanches imply maximum dynamic range in cortical networks at criticality. J. Neurosci. 29, 15595–15600.
Shew, W.L., Yang, H., Yu, S., Roy, R., Plenz, D., 2011. Information capacity and transmission are maximized in balanced cortical networks with neuronal avalanches. J. Neurosci. 31, 55–63.
Shi, W., Shang, P., Ma, Y., Sun, S., Yeh, C.H., 2017. A comparison study on stages of sleep: quantifying multiscale complexity using higher moments on coarse-graining. Commun. Nonlinear Sci. Numer. Simul. 44, 292–303.
Shimaoka, D., Song, C., Knöpfel, T., 2017. State-dependent modulation of slow wave motifs towards awakening. Front. Cell. Neurosci. 11, 108.
Song, C., Piscopo, D.M., Niell, C.M., Knöpfel, T., 2018. Cortical signatures of wakeful somatosensory processing. Sci. Rep. 8, 11977.
Stein, R.B., Gossen, E.R., Jones, K.E., 2005. Neuronal variability: noise or part of the signal? Nat. Rev. Neurosci. 6, 389.
Takahashi, T., Cho, R.Y., Murata, T., Mizuno, T., Kikuchi, M., Mizukami, K., et al., 2009. Age-related variation in EEG complexity to photic stimulation: a multiscale entropy analysis. Clin. Neurophysiol. 120, 476–483.
Takahashi, T., Cho, R.Y., Mizuno, T., Kikuchi, M., Murata, T., Takahashi, K., Wada, Y., 2010. Antipsychotics reverse abnormal EEG complexity in drug-naive schizophrenia: a multiscale entropy analysis. Neuroimage 51, 173–182.
Takahashi, T., 2013. Complexity of spontaneous brain activity in mental disorders. Prog. Neuro-Psychopharmacol. Biol. Psychiatry 45, 258–266.
Vakorin, V.A., Lippé, S., McIntosh, A.R., 2011. Variability of brain signals processed locally transforms into higher connectivity with brain development. J. Neurosci. 31, 6405–6413.
Wang, D.J., Jann, K., Fan, C., Qiao, Y., Zang, Y.F., Lu, H., Yang, Y., 2018. Neurophysiological basis of multi-scale entropy of brain complexity and its relationship with functional connectivity. Front. Neurosci. 12, 352.
Yang, A.C., Wang, S.J., Lai, K.L., Tsai, C.F., Yang, C.H., Hwang, J.P., et al., 2013. Cognitive and neuropsychiatric correlates of EEG dynamic complexity in patients with Alzheimer's disease. Prog. Neuro-Psychopharmacol. Biol. Psychiatry 47, 52–61.
Yang, A.C., Huang, C.C., Liu, M.E., Liou, Y.J., Hong, C.J., Lo, M.T., et al., 2014. The APOE ε4 allele affects complexity and functional connectivity of resting brain activity in healthy adults. Hum. Brain Mapp. 35, 3238–3248.
Yang, D.P., Zhou, H.J., Zhou, C., 2017. Co-emergence of multi-scale cortical activities of irregular firing, oscillations and avalanches achieves cost-efficient information capacity. PLoS Comput. Biol. 13, e1005384.
Zhang, H.Y., Wang, S.J., Liu, B., Ma, Z.L., Yang, M., Zhang, Z.J., Teng, G.J., 2010. Resting brain connectivity: changes during the progress of Alzheimer disease. Radiology 256, 598–606.